

Source Mergers and Bubble Growth During Reionization

J. D. Cohn^{a,b} and Tzu-Ching Chang^{y,b}

^aSpace Sciences Laboratory,

^bTheoretical Astrophysics Center, Dept. of Astronomy,
University of California, Berkeley, CA 94720

March 7, 2019

Abstract

The recently introduced models of reionization bubbles based on extended Press-Schechter theory (Furlanetto, Zaldarriaga & Hernquist (2004a)) are generalized to include mergers of ionization sources. Sources with a recent major merger are taken to have enhanced photon production due to star formation, and accretion onto a central black hole if a black hole is present. This produces a scatter in the number of ionized photons corresponding to a halo of a given mass and a change in photon production over time for any given halo mass. Photon production histories, bubble distributions, and ionization histories are computed for several different parameter and recombination assumptions; the resulting distributions interpolate between previously calculated limiting cases.

1 Introduction and Background

Reionization marks the historical event when hydrogen in the universe transformed from mostly neutral to mostly ionized; it has only recently become accessible via observations and numerical simulations and has stirred great interest and advances in our understanding of early structure formation (see e.g. reviews by Barkana & Loeb (2001), Loeb & Barkana (2001), Cooray & Barton (2006), Loeb (2006)).

Current observations suggest that the process of reionization is complex, perhaps lasting over an extended period of time (for a review, see Fan, Carilli

^jjohn@berkeley.edu

^ytchang@astron.berkeley.edu

& Keating (2006)). The optical depth to electron scattering seen by WMAP (Spergel et al (2006)) can be modeled with reionization starting by $z \approx 10$. On the other hand, spectroscopic observations of high-redshift quasars and Gunn-Peterson absorption due to intervening neutral hydrogen in the intergalactic medium (Becker et al (2001), Fan et al (2003), White et al (2005)), although with significant fluctuations along different lines of sight (Oh & Furlanetto (2005)), which suggests that the tail end of reionization occurs at $z \approx 6$.

Theoretically, questions about reionization range from the fundamental timeline of reionization to detailed characteristics. The latter include the nature of ionizing sources, the topology of the ionized regions and their evolution, and the behavior of the ionized regions relative to matter overdensities and voids. Numerical approaches (e.g. Gnedin (2000), Razoumov et al (2002), Ciardi, Stoehr & White (2003), Sokasian et al (2003; 2004)) are fruitful due to the complex nature of the sources and nonlinear clustering involved. For small regions, simulations can track the nonlinear effects, although much known physics is too difficult to incorporate, and much unknown physics remains. However, the large disparity in size between the ionized regions (which can grow to be tens of Mpc comoving, e.g. Wyithe & Loeb (2004), Furlanetto, Zaldarriaga & Hernquist (2004a)) and the small scale distributions and physics of sources producing the photons is difficult to capture in a simulation. Recent numerical simulations have just begun to combine large and small scale effects in larger volumes (see for instance Kohler, Gnedin & Hamilton (2005), Iliev et al (2005)).

Analytic models are useful to encompass the wide range of scales in order to try to identify generic behavior. In addition, analytic models allow exploring a larger range of parameters and other assumptions. This paper extends an analytic model introduced by Furlanetto, Zaldarriaga and Hernquist (2004a) (hereafter FZH) to characterize the growth of ionized regions or bubbles. The basic idea is to move beyond the initial step of considering H II regions around individual collapsed halos (e.g. Arons & Winberg (1972), Barkana & Loeb (2001)) to consider regions around several collapsed halos. The simplest form goes as follows: collapsed halos of mass M are able to ionize a mass M_{ion} where

$$M_{\text{ion}} = \alpha M \quad (1)$$

and α is a constant. Halos need to be massive enough to produce photons, thus $M > m_{\text{min}}(z) = m(T = 10^4 \text{K}; z)$ is imposed, i.e. they need to be massive enough to have efficient atomic Hydrogen line cooling. For a constant α , independent of m , the size of ionized regions can be calculated immediately in closed form: an ionized region of mass M_{ion} has the fraction of mass f_{coll} bound in halos above $m_{\text{min}}(z)$ equal to or greater than α^{-1} . Using extended Press-Schechter theory (references below), the mass fraction f_{coll} in a fully

ionized bubble of mass M then obeys

$$f_{\text{coll}} = \text{erfc} \left[\frac{\rho_c(t) M}{2 (\rho_{\text{min}}^2 M)} \right] > 1 : \quad (2)$$

This constrains the average overdensity $\bar{\rho}_M$ for any M . Here ρ_{min} denotes the density fluctuations smoothed on a scale of mass $m_{\text{min}}(z)$, likewise for $\rho^2(M)$, and $\rho_c(t)$ is the threshold density for collapse. The overdensity required for collapse is $\rho_c = 1.686$, in this picture the densities stay constant and the threshold lowers with time, so $\rho_c(t) = \rho_c D(z(t))$ where $D(z)$ is the growth factor. The bubble's average overdensity relative to $\rho_c(t)$ is $\bar{\rho}_M$, corresponding to physical overdensity $\bar{\rho}_{R,M}(t) = \bar{\rho}_M D(z(t))$, and $V_M (1 + \bar{\rho}_{R,M}(t)) = M$, where V_M is the bubble volume and $\bar{\rho}$ is the mean density. The condition for a bubble to be ionized, equation 2, can be rewritten in a form that is more easily generalizable,

$$f_{\text{coll}} = 1 : \quad (3)$$

The function $\bar{\rho}_M$ allows one to determine the number distribution of bubbles of mass M and other properties discussed below.

In FZH, recombinations were included implicitly in . A more sophisticated approach balancing the total number of ionizations and recombinations per unit time in the intergalactic medium (IGM) was introduced in Furlanetto & Oh (2005) (hereafter FO05), where they considered two models of IGM gas density distribution for recombinations: one model adopted an analytical fit of gas density to simulations at low redshift by Miralda-Escude, Haehnelt & Rees (2000), and extrapolated it to high z ; a second model considered minihalos as photon sinks. Minihalos are neutral, dense blobs with mass $10^6 M_\odot$, randomly distributed in the IGM.

These results were extended by Furlanetto, Miquinn & Hernquist (2005) (hereafter FMH05) and others. For example, FMH05 include the effects of different halo mass functions, a mass dependent $\bar{\rho}_M$, and stochastic fluctuations in the galaxy distribution. They found the consequences of these additional effects on the bubble size distributions and corresponding evolution in time, the emissivity inside a bubble, the observable neutral hydrogen 21 cm power spectra, and the kinetic Sunyaev-Zeldovich signal. Tools for calculations of the latter were developed by Zahn et al (2005) and Miquinn et al (2005a), they also extended many aspects of the approach. Other consequences of this model for observables have been calculated, for example in Furlanetto, Hernquist & Zakarriaga (2004), Furlanetto, Zakarriaga & Hernquist (2004b; 2006), Miquinn et al (2005b) and Alvarez et al (2005).

Here we extend this model further to include the effects of major mergers. The original models are based on a time independent $\bar{\rho}_M$ which only depends upon mass. Halos which have recently had a major merger produce an increased number of photons, due to starbursts (1.25 halo mass ratios)

or induced black hole accretion (1:10 halo mass ratios). Consequently major mergers introduce a time dependence in the average of τ and a scatter in τ . We expect halo major mergers to be important, as even the smallest objects producing photons (chosen to be those with $T > 10^4 \text{K}$) have masses several orders of magnitude above M_{min} at high redshifts, and thus are highly biased and very actively merging. We use a "microphysics" estimate of photon emission due to quiescent star formation, merger induced starbursts and black hole accretion. As the microphysics models have many unknowns, we are especially interested in features which characterize the merging itself rather than the details we choose.¹

There are several related studies in this active area of research. This is not the mergers of the bubbles, which was already considered in F005 and it is not the scatter (Furlanetto et al (2005)) in τ due to the stochasticity of the number of collapsed halos (Barkana & Loeb (2004a), Babich & Loeb (2005)), or the difference between metal rich and metal poor regions (Barkana & Loeb (2005)). Other related work includes the calculation of the effects of mergers in producing cumulative number of photons by quasars up to redshifts $z \leq 5$, e.g. by Wyithe & Loeb (2002) and Madau et al (2004). Here we want the effects of the mergers in producing a time dependent photon production rate, with scatter, for collapsed halos of a given mass, and the consequences for the enclosing bubbles.

Section 2 gives the analytic framework and formulae for the merger rates, recombinations and scatter. The natural quantity to use is the instantaneous photon production rate which then determines the time derivative of τ rather than τ itself. This leads to a natural interpolation between limits considered in earlier work; the total number of ion present is found by integrating the photon production rate over time, and subtracting recombinations. Three prescriptions for recombinations are used. The scatter requires additional assumptions, we describe and choose a simple case next. In section 3, we calculate the analytic form of the time derivative $\dot{\tau}$ in terms of the star formation and black hole accretion parameters and then explicitly show its dependence upon mass and redshift for a few examples. Section 4 shows the effects on bubbles using a fiducial model and some variations: the bubble overdensity δ_M as a function of bubble mass M (as a function of redshift and initial conditions), the characteristic bubble sizes and ionization fractions over time x_i , and the bubble size distributions associated with the (major) merger scatter. Section 5 concludes. An appendix spells out the basic Extended Press-Schechter quantities, details the estimates used to find the minimum halo mass for a black hole to be present and describes some other possible assumptions for scatter.

¹ Ideally this could eventually be turned around to constrain the "microphysics" but it is not clear how constraining that might be given the vast uncertainties.

2 Analytic Framework

In this section we describe the analytic calculations, assumptions and formulae used in the rest of the paper: the halo mass function, major merger rates, recombinations and the merger related scatter. The input parameters to our calculations are $\sigma_8 = 0.3$; $\sigma_8 = 0.7$; $\sigma_8 = 0.9$; $\sigma_8 h^2 = 0.02$ a scale invariant initial power spectrum $n = 1$, and the Eisenstein-Hu (1997) transfer function. In order to get some idea of the effect of a change of cosmology, we also considered $n = 1.05$ which enhances fluctuations for large k , i.e. small scales, and $\sigma_8 h^2 = 0.225$. Masses are defined in terms of $h^{-1} M_\odot$ and all lengths are comoving.

2.1 Halo Mass Function

The starting point for the extended Press-Schechter bubble model of reionization is the number density of collapsed halos of dark matter. We use the Press-Schechter formalism (1974) to estimate numbers and source major merger rates. Examples of the resulting number densities and properties have been detailed by Barkana & Loeb (2001) and Mo & White (2002).

Our use of the Press-Schechter mass function warrants some discussion. The Sheth-Tormen (2002) mass function is a better fit to simulations at low redshifts; mass functions found in high redshift simulations (Jang-Condell & Hernquist (2001), Reed et al (2003), Heitmann et al (2006), Iliev et al (2005)) often lie between Sheth-Tormen and Press-Schechter (the best agreement for Heitmann et al was with the fitting function of Warren et al (2005)). Agreement with dark matter simulations is not necessarily indicative of appropriateness either, as baryons and dark matter are not as tightly coupled at high redshifts (e.g. Naoz & Barkana (2005), Bagla & Prayad (2006)). For the original model (which we modify here), the effect of using the Sheth-Tormen mass function instead of the Press-Schechter mass function for the number of sources was seen to be small (Furlanetto et al (2005)). We altered the "tilt" n in one set of runs from $n = 1$ to $n = 1.05$ to see the effect of increased small scale structure as found in these simulations.

The Press-Schechter mass function is the most tractable and our interest is in trends rather than exact numbers. With it, the number of recently merged halos can be calculated easily using extended Press-Schechter theory (Bond et al (1991), Lacey & Cole (1993; 1994), Bower (1991), Kitayama & Suto (1996)).² There are problems as well with extended Press-Schechter theory, especially when considering large mass ratios in merger rates (see Benson et al (2005) for a recent discussion of this). We restrict ourselves to

²These are actually formulae for fast mass gain and can include accretion. Analytic formulae differentiating between major mergers and accretion have been found by Raig et al (1998), Salvador-Sole et al (1998) and Andreu et al (2001).

major mergers, with small mass ratios. In addition to being in the regime where extended Press-Schechter works the best, this allows predecessors and final halos to be identified uniquely (a halo only has one predecessor with mass greater than half the final halo mass).

2.2 Photon Sources

2.2.1 Major Merger Rates

After a major merger, a halo produces extra photons for some specified amount of time, denoted t_{ion} . We are interested in the number of halos of a given mass which are still "active," i.e. which are still producing extra photons due to a recent major merger. We ignore the lag between the actual merger and the beginning of the photon production, which should not change the general trends of interest. We also assume that the extra photon production rate is constant during t_{ion} after the merger, so that we do not care about when exactly the merger happened, only that it happened within this relaxation time.

The number of recently merged halos with mass m at time t is the product of two factors, depending upon two times: the time of the merger t_i and the subsequent time of observation t , where the latter is close enough to t_i for the halo to still be excited from the merger, i.e. $t - t_i < t_{\text{ion}}$. The first factor is the fraction of halos that have mass m_0 which have jumped at time t_i from mass m_i , $P_1(m_i \rightarrow m_0; t_i) \frac{m_0}{m_i} dm_i dt_i$. (The overdot denotes derivative with respect to t_i .) The factor of $m_0 = m_i$ converts from the number of points in such halos to the number of such halos. We then want this "excited" halo of mass m_0 to be in a halo of mass m at time t . The probability that a point in a halo of mass m at time t was in a halo of mass m_0 at time t_i is $P_1(m_0; t_i | n; t) dm_0$. Formulae for P_1 and its derivative are in the appendix.

For bubbles we need to go one step further and consider the regions of mass M surrounding these mass m sources. The probability that a halo (bubble) of mass M and overdensity δ_M contains a halo of mass m at time t is denoted by $P_1(m; t | M; \delta_M) dm$, corresponding to a number density of halos $n(m; t | M; \delta_M) dm = \frac{1}{m} P_1(m; t | M; \delta_M) dm$. (When a time t rather than δ is written as an argument of P_1 the implicit assumption is that one uses $\delta_c(t)$ in P_1 , the threshold density corresponding to time t .) Thus the number of halos which have merged at time t_i from mass m_i to mass m_0 and are in a halo of mass m at time t within a bigger halo (bubble) of mass M and overdensity

n_M is given by³

$$V_M n(m; t; M; M) P_1(m_i; m_0; t_i) P_1(m_0; t_i; j_n; t) \frac{m}{m_i} dm dt_i dm_i dm_0 : \quad (6)$$

2.2.2 Total Photon Rates

The rate photons are produced in a region with mass M and overdensity M is the number of additional photons due to the mergers, plus the quiescent number of photons due to the collapsed halos present even if no merger has occurred. (We assume that each photon produced corresponds to an ionization in the region, in principle the bubble region can have some "escape fraction" which would effectively lower the number of ionizations in a region relative to the number of photons produced.) A constant lifetime T gives a $\tau_t = T$. More generally, there is a dependence upon the mass of the initial and final masses before the merger ($m_i; m_0$), the mass m at the time of interest, and $t_i; t$ to give $\tau_t(m_i; m_0; t_i; m; t)$. The quiescent rate is taken to be $\tau_{qj}(m)$. These quiescent photons are from stars not created during starbursts, i.e. ongoing star formation, in part due to accretion. Putting this together to get the rate mass is ionized gives

$$\begin{aligned} R & \int dm n(m; t; M; M) \frac{m}{m_i} \\ f & \int_R dt_i dm_i dm_0 \tau_t(m_i; m_0; t_i; m; t) P_1(m_i; m_0; t_i) P_1(m_0; t_i; j_n; t) \frac{m}{m_i} + \tau_{qj}(m) g \\ = & \int dm n(m; t; M; M) \frac{m}{m_i} \tau_{ja}(m) \\ = & (f)_t \end{aligned} \quad (7)$$

The above defines $(f)_t$ and $\tau_{ja}(m)$. Section 3 derives estimates for $\tau_t(m_i; m_0; t_i; m; t)$ using models for star formation and black hole accretion, and gives parameters and limits for the integrals. In the integrals, the mass limits are determined by the mass ratio criteria for major mergers. In all

³This can be written in a more intuitive way. The number of merged halos is the fraction of recently merged halos of mass m_0 at t_i times the number $n(m_0; t_i)$ of $m_0; t_i$ halos. Multiplying by their survival probability $P_2(m; t; j_n; t_i)$ of surviving to $m; t$ gives the number at $m; t$, and the recently merged fraction is found by dividing by $n(m; t)$. This fraction of the $m; t$ halos found in a bubble of mass $M; M$ requires multiplying by the number of $m; t$ halos in $M; M$, $n_h(m; t; M; M) = \frac{1}{m} P_1(m; t; M; M)$ to give a number density. This is

$$P_1(m_i; m_0; t_i) \frac{m_0}{m_i} n(m_0; t_i) P_2(m; t; j_n; t_i) \frac{1}{n(m; t) m} = P_1(m; t; M; M) \quad (4)$$

which equals the above because

$$P_1(m_0; t_i; j_n; t) n(m; t) \frac{m}{m_0} dm_0 dm = P_2(m; t; j_n; t_i) n(m_0; t_i) \frac{m_0}{m} dm_0 dm \quad (5)$$

(also this can be used to get an explicit expression for P_2).

cases we require $m_{i, \max} = m_0 > m_i = m_0 > 0.5$. The lower limit means some major mergers are neglected, but ensures that no major merger is counted twice, as only one halo with $m_i > m_0 = 2$ can end up in m_0 . This is thus a lower limit on the number of mergers. The time limits in the integrals are determined by the time scales of relaxation after the mergers. Both the mass and time limits can differ for starbursts and black hole accretion.

In principle $m_{0, \min}$ can be as small as $m(T = 10^4 \text{K}; z) = \frac{2.04 \cdot 10^9}{(1+z)^{3-2}} h^{-1} M_\odot$. However the probabilities above double count a halo which has two mergers within a relaxation time, which is more likely if $m_{0, \min}$ is chosen to be small. For the number of photons contributed, this is perhaps accurate (but perhaps not, e.g. for starbursts there might be gas missing after the first merger for some period of time). However for the scatter it will give two halos with recent mergers rather than just the one which had two mergers. However, if $m_{0, \min}$ is taken to be too large, the number of photons will be undercounted and the scatter underestimated. We used both $m_{0, \min} = 0.1m$ and $m_{0, \min} = m_{\min}(T = 10^4 \text{K}; z)$ in our calculations,⁴ for nontrivial mass dependence of star formation (referred to as $\beta = 2=3$ below) these two choices are essentially indistinguishable.

The ionized mass fraction in a region of mass M with overdensity $\bar{\rho}_M$, the generalization of equation 3, is then

$$\int dt [(f)_t - R_{\text{recomb}}(R_{\text{ion}}(M); \bar{\rho}_M; t)] : \quad (11)$$

where $R_{\text{recomb}}(t)$ is the instantaneous recombination rate in the bubble volume, depending upon $R_{\text{ion}}(t)$, the effective radius of the ionized region at this time. The dependence upon R_{ion} takes into account that not all regions inside a bubble at time t are ionized at earlier times: recombinations can only occur where there are ions already present. As the first term gives the total number of photons produced in the region, assumed to produce the same number of ions, recombinations can be directly subtracted off.

⁴If we take the limits of m_0 to be independent of m , then the integral over m can be done explicitly using an identity for composing the probabilities. This gives the mass fraction which had mergers at t_i to mass m_0 in a halo of mass M as

$$\int dm P_{\pm}(m_i | m_0; t_i) \frac{m}{m_i} P_{\pm}(m_0; t_i | m; t) P_{\pm}(m; t | M; \bar{\rho}_M) dm_i dm_0 dt_i \quad (8)$$

$$= P_{\pm}(m_i | m_0; t_i) \frac{m}{m_i} P_{\pm}(m_0; t_i | M; \bar{\rho}_M) dm_i dm_0 dt_i \quad (9)$$

$$(10)$$

ie. it doesn't matter what halo the original m_0 halo is in at time t , just that it is in the bubble M .

2.3 Recombination

Recombinations decrease the number of ions present. We use the two estimates for the recombination rate for an ionized region of radius $R_{\text{ion}}(t)$ and overdensity δ_M chosen by FO05 and a third by Mellina et al (2006). The recombination rate per hydrogen atom inside a region of radius R_{ion} at time t and overdensity δ_M is

$$A(T)n_e C(R_{\text{ion}}(t)) = A_u (1 + \delta_{RM}(t)) C(R_{\text{ion}}(t)); \quad (12)$$

where $n_e = n_e (1 + \delta_{RM}(t))$. The physical overdensity $\delta_{RM}(t)$ enhances the rate at mean density $A_u = A(T)n_e = 2.4 \times 10^6 \text{ yr}^{-1}$. (We use $A(T = 10^4 \text{ K})$ for case A recombination, case B recombination (optically thick) takes $A_u \approx 0.6 A_u$.) The three recombination models have different clumping factors, described in subsections below.

To go from the ionization rates per hydrogen atom in the bubble to the change in ionization fraction in equation 11 requires the comparison of counts⁵. The ionized mass fraction times the hydrogen mass of the bubble gives the number of ions in the bubble at a given time. The recombination rate at the same time is the rate per hydrogen atom times the number of ionized hydrogen atoms, $n_h (1 + \delta_{RM}(t)) V_{\text{ion}}$. Dividing by the total mass of the bubble and noting $V_{\text{ion}} = \frac{M_{\text{ion}}}{M (1 + \delta_{RM}(t))}$, the resulting ionization fraction with recombinations included, at some time t , is

$$z_t \frac{d f_{\text{ion}}}{dt} = A_u \frac{M_{\text{ion}}(t^0)}{M} (1 + \delta_{RM}(t^0)) C(R_{\text{ion}}(t^0)); \quad (13)$$

The mechanics of doing this integral are discussed in section 4, we now describe the clumping factors $C(R_{\text{ion}})$ for the three different recombination models.

2.3.1 The MHR model

The first model (hereafter called the MHR model) is a smooth IGM gas distribution of Miralda-Escude, Haehnelt & Rees (2000). They use the volume density distribution of IGM gas, $P_V(\delta)$ ($\delta = \delta_M$) to simulations at $z = 2-4$, finding

$$P_V(\delta) d\delta = A_0 \exp\left[-\frac{(\delta - 3)^2 C_0^2}{2(\delta_0 - 3)^2}\right] d\delta \quad (14)$$

with $\delta_0 = 2.5$. A_0 and C_0 are set by requiring mass and volume normalization and δ_0 is the variance of density fluctuations smoothed on the Jeans scale for an ionized medium (at higher z , $\delta_0 = 7.61 = (1 + z)$ to better than 1%). The

⁵We thank S. Furlanetto for discussions about this

distribution $P_V(z)$ is taken to be independent of environment (rather than depending upon M). For recombination, they assume all gas below some density threshold $< z_i$ is ionized and everything above is shielded. One finds z_i by noting that recombination limits bubble growth (i.e. the mean free path $\lambda_i = \lambda_0 [1 - F_V(z_i)]^{-2=3}$ is the radius of the ionized region R_{ion} . Here $\lambda_0 H(z) = 60 \text{ km s}^{-1}$ (in physical units) and $F_V(z_i)$ is the fraction of volume with $< z_i$. (If the region's radius $R_{\text{ion}} < \lambda_0$ then the assumption is that recombination is negligible and z_i is set to zero.) The factor C is then

$$C_{\text{MHR}}(R_{\text{ion}}) = \int_0^{z_i} dz P_V(z)^{-2}; \quad (15)$$

again, note R_{ion} enters implicitly via $z_i(R_{\text{ion}})$. At large R_{ion} $C_{\text{MHR}}(R_{\text{ion}})$ tends to asymptote to a constant, and for most (all) radii it is smaller than $C_{\text{mh}}(R_{\text{ion}})$ (C_{MIPS}) described below.

2.3.2 M inihalos

The second model is a minihalo model of small dense absorbing clumps, taken to have mass of $M_{\text{mh}} = 10^6 M_\odot$ with comoving mean free path

$$\lambda_{\text{mh}} = \frac{1}{n_{\text{mh}} R_{\text{mh}}^2} = 15.7 h \left(\frac{M_{\text{mh}}}{10^6 M_\odot} \right)^{-1=3} \left(\frac{0.05}{f_{\text{mh}}} \right) \left(\frac{h}{18} \right)^{2=3} \left(\frac{h^2}{0.15} \right)^{-1=3} h^{-1} \text{ Mpc} \quad (16)$$

and

$$C_{\text{mh}}(R_{\text{ion}}) = (1 - f_{\text{mh}})^2 \exp(R_{\text{ion}} = \lambda_{\text{mh}}) \quad (17)$$

where $f_{\text{mh}} = 0.05$ is the mass fraction taken to be in minihalos. Unlike the other two models it is redshift independent. Note that the effect of minihalos on recombination and thus reionization is likely to be more complicated than this simple prescription, which is probably an overestimate (Iliev, Scannapieco & Shapiro (2005), Ciardi et al (2006)).

2.3.3 The MIPS model

A third prescription from clumping, matched to numerical simulations is by Mellema, Iliev, Pen & Shapiro (2006) (MIPS), which is an improvement for the IGM clumping factor to the one given by Iliev et al (2005). They used a N -body simulation with a $3.5 h^{-1} \text{ Mpc}$ box and 3248^3 particles to get a mass resolution down to the Jeans mass; they then took out all found halos, including minihalos, to eliminate their contributions to the IGM density field. The resulting IGM was fit to give an R_{ion} independent clumping factor:

$$C_{\text{MIPS}} = 27.466 \exp(0.114z + 0.001328z^2) \quad (18)$$

It resembles the MHR clumping factor at large R_{ion} as the former asymptotes to a constant for large R_{ion} and high z , but is larger numerically, and thus

more effective at suppressing bubble formation than the MHR model. This will be referred to as the MIPS model in the following.

2.4 Scatter

Extended Press-Schechter gives the fraction of halos which have had recent mergers. This is an average quantity, just as the number of collapsed halos in a larger region of mass M is given only on the average by $n(m; t_M; M)$. In any region a scatter in the number of sources will lead to a scatter the number of ionizing photons and thus in bubble sizes. For $n(m; t_M; M)$, FMH05 took the scatter due to the stochastic nature of the collapsed halo distribution (halos of mass m) in the larger bubbles of mass M to be Poisson. Numerical simulations have found this scatter to be within a factor of two of Poisson for the cases studied by Sheth & Lemson (1999) and Casa-Miranda et al (2002). In equations, the ionized mass fraction is

$$\int dm \frac{m}{M} n(m; t_M; M) \quad (19)$$

and they assumed for the scatter

$$\ln \langle n(m; t_M; M) n(m^0; t_M; M) \rangle_i = n(m; t_M; M) n(m^0; t_M; M) + \frac{\delta_D(m - m^0)}{V_M} n(m; t_M; M); \quad (20)$$

where δ_D is a Dirac delta function.

For our case we want the scatter of

$$\int dt \int dm \frac{m}{M} n(m; t_M; M) \frac{m}{t_{ja}(m)}; \quad (21)$$

i.e.

$$\int dt \int dm \int dm^0 \frac{m m^0}{2} \ln \langle n(m; t_M; M) \frac{m}{t_{ja}(m)} n(m^0; t^0_M; M) \frac{m^0}{t^0_{ja}(m^0)} \rangle_i; \quad (22)$$

Thus instead of the scatter of $n(m; t_M; M)$ for fixed time above, we need

$$\ln \langle n(m; t_M; M) n(m^0; t_M; M) \rangle_i; \quad (23)$$

In addition, $t_{ja}(m)$ has scatter. To our knowledge the appropriate distributions have not been calculated in numerical simulations, and thus additional assumptions are required to continue.

The simplest assumption is to take the distribution of $n(m; t_M; M)$ to be Poisson both in mass and in time:

$$\ln \langle n(m; t_M; M) n(m^0; t^0_M; M) \rangle_i = n(m; t_M; M) n(m^0; t^0_M; M) + \frac{1}{V_M} \delta_D(m - m^0) \delta_D(t - t^0) n(m; t_M; M) \quad (24)$$

Note that n is a function of t only through $\ell(t)$ and thus $\ell(t)$ is taken to be the argument of the Dirac delta function. Using $\delta(t - t^0)$ would give the wrong dimensions.

The second assumption is for the scatter of

$$\int_{t_{ja}}^Z dt_i dm_i dm_0 t(m_i; m_0; t_i; m; t) P_{-1}(m_i! m_0; t_i) P_1(m_0; t_i; jn; t) \frac{m}{m_i} + t_{jq}(m) : \quad (25)$$

We define $n^a(m_0; jn; t)$ which appears in $t_{ja}(m)$ the following way:

$$\int_{t_{ja}}^Z dt_i dm_i t(m_i; m_0; t_i; m; t) P_{-1}(m_i! m_0; t_i) \frac{m_0}{m_i} P_1(m_0; t_i; jn; t) = \int_{a=1}^X \frac{m_0}{m_i} n^a(m_0; jn; t) t^a(m_0) : \quad (26)$$

The number density $n^a(m_0; jn; t)$ counts the recently merged halos of mass m_0 in a halo of mass m , with the index a denoting the range of integration for $m_i; t_i$. There are three ranges, corresponding to starbursts, black hole accretion or both. For each $t(m_i; m_0; t_i; m; t)$ only depends on which of these three cases is at hand and the value of m_0 , and so it is denoted $t^a(m_0)$. The Poisson assumption for $n^a(m_0; jn; t)$ is then

$$n^a(m_0; jn; t) n^b(m_0^0; jn; t) i = \frac{(m_0 \quad m_0^0)}{V_m} n^a n^b(m_0; jn; t) \quad (27)$$

There is also an assumption being made that the number with scatter is related to the product of $P_{-1} P_1$, rather than a separate scatter for the merger rate to mass m_0 and then scatter for the inclusion of these m_0 halos in m .

The full scatter is then

$$\begin{aligned} & h_{t_{ja}}(m) n(m; t; M; M) t_{ja}^0(m^0) n(m^0; t^0; M; M) i \\ & = \int_{t_{ja}}^Z dt_i dm_i dm_0 t(m_i; m_0; t_i; m; t) P_{-1}(m_i! m_0; t_i) P_1(m_0; t_i; jn; t) \frac{m}{m_i} \\ & + \frac{1}{V_M} D(m \quad m^0) D(\ell(t) \quad \ell(t^0)) n(m; t; M; M) h_{t_{ja}}^2(m) i \\ & = \frac{1}{R^M} D(m \quad m^0) D(\ell(t) \quad \ell(t^0)) n(m; t; M; M) f_{t_{ja}}^2(m) \\ & + \int_{t_{ja}}^Z dt_i dm_0 dm_i dt_i (1 + R(t; t_i)) t(m_i; m_0; t_i; m; t) m^2 \frac{1}{m m_i} P_{-1}(m_i! m_0; t_i) P_1(m_0; t_i; jn; t) g \end{aligned} \quad (28)$$

Here $m = (1 + R(t; t_i)) V_m$ was used, where $R(t; t_i)$ is the physical overdensity $\ell(t) D(z(t_i))$ and the combination $\int_{t_{ja}}^Z dt_i dm_i dm_0 t(m_i; m_0; t_i; m; t)$ was pulled out.

We then define the scatter in $\int dt (f)_t$ via

$$\left(\int dt (f)_t \right)^2 = \int dt dt^0 (f)_t (f)_{t^0} i = \int dt (f)_t i \int dt^0 (f)_{t^0} i \quad (29)$$

We calculated the consequences of this simplest set of assumptions for our models; some other possibilities are described in the appendix.

The scatter is an integral over time. In practice we cannot integrate back to arbitrarily early times, and so an initial condition and initial scatter are needed. See below for discussion.

3 Photon increase from mergers

The analytic expressions above require estimates of $\dot{t}(m_i; m_0; t_i; m; t)$ and the quiescent rate $\dot{t}_q(m)$ to give concrete results. The two main sources of extra photons due to a major merger are starbursts and, if a central black hole is present, accretion onto a central black hole (Kaumann & Haehnelt (2000), Cavaliere & Vittorini (2000)). Merger induced star formation and black hole accretion at high redshift might differ from their low redshift counterparts, detailed calculations and simulations have not yet been done. We use low redshift calculations and measurements as a guide. We stress that we are most interested in the effects of the time dependence, as the unknowns of the detailed modeling are vast.

A major merger to a halo of mass m will add a total number of photons $N(m)$ over a time t_{ion} . These N photons can ionize the hydrogen in a region with mass M obeying $N = \frac{M}{m_p} \frac{bX}{m}$ where $X = 0.76$ and m_p is the proton mass. This is the amount of mass M that can be ionized over the whole time T , giving, if $M = m$,

$$= \frac{N}{m} \frac{m_p}{X} \left(\frac{b}{m}\right)^{-1} \quad (30)$$

We will want to compare the contributions to photons at some given time, thus we will look at all the photons being contributed assuming a constant production rate, i.e. $\dot{t} = \frac{N}{t_{\text{ion}}}$. The times t_{ion} for black hole accretion and starbursts differ in general.⁶

3.1 Star Formation and Starbursts

Photon production due to star formation can be estimated via (e.g. Loeb, Barkana & Hernquist (2005))

$$\frac{dN_{\text{stars}}}{dt} = \frac{m}{m_p} \frac{b}{m} \frac{N_{\text{ion}}}{t} \quad (31)$$

leading to

$$\dot{t}(m_i; m_0; t_i; m; t) = \frac{1}{X} \frac{N_{\text{ion}}}{t} (\text{stars}) \quad (32)$$

We assume that the starbursts change the rate from a constant quiescent rate to a constant starburst rate for a time $t + t_{\text{burst}}$, until the stars due to the starburst are gone.⁷

⁶More accurately, the accretion onto a black hole, if Eddington as is commonly assumed, tends to increase with time until all the infalling material is gone, while the starbursts tend to decay with time until all the gas is gone. However other estimates of black hole accretion have the accretion also slow down with time as the gas supply is decreased.

⁷Note that the photon production rate estimate in FO05 and in FMH05 has time independent, and assumes that all mass going above 10^4K is instantaneously converted into photons, which is another common approximation, e.g. Somerville & Livio (2003).

For N_{ion} our parameters are similar to Loeb et al (2005). We take a star lifetime $t = 80 \text{ M yr}$. Showing our choices in parentheses⁸, the efficiency with which baryons are incorporated into stars is $f (= 0.1)$, and each baryon in a star produces $N_{\text{bary}} (= 4400)$ photons, with $f_{\text{esc}} (= 0.05)$ of them escaping. Combining these we get

$$\begin{aligned} N_{\text{ion}} &= N_{\text{bary}} f f_{\text{esc}} & m > m_{\text{ref}}(z) \\ &= N_{\text{bary}} f f_{\text{esc}} \left(\frac{m}{m_{\text{ref}}(z)} \right) & m < m_{\text{ref}}(z) \end{aligned} \quad (33)$$

The power $= 2=3$ is to take into account the scaling of star formation found in low stellar mass galaxies (below $m_{\text{stellar}} = 3h^{-1} 10^{10} h^{-1} \text{ M}_{\odot}$) by Kauffmann et al (2003), we assume that it is the same for both starbursts and quiescent star formation as in the $z = 0$ sample low mass halos are not merging very often. We will call this scale m_{ref} in the following, our choices for it are discussed below.

With a starburst, f will be larger (more gas will go into baryons) for a time $t_{\text{burst}} + t$ (that is, after the merger the number of baryons going into stars will increase, and these stars will add extra photons for their entire lifetime). The average f_{burst} at this time is $f_{\text{burst}} = (t_{\text{burst}} + t)$. Simulations of mergers at low redshifts provide some suggestions for f for a starburst, e.g. a range of 65% – 85% of the total gas (Mihos & Hernquist (1994; 1996)) or 80% of the cool gas (Springel, Di Matteo and Hernquist (2005)) going into stars (see also the studies of gas available at early times by Machacek, Bryan & Abel (2003)). Observationally, starburst star formation is t by a decaying exponential with time scales as short as 20 M yrs in some examples but lasting up to hundreds of M yrs (e.g. Papovich, Dickinson & Ferguson (2001), Shapley et al (2001), Conselice (2006)) with similar time ranges used to analyze observed samples (Kauffmann et al (2003)).

We only consider Pop II stars, although it would be straightforward to generalize beyond this in our formalism. The transition redshift between creating Pop III stars and creating Pop II stars has been estimated to be $z = 15$ (Yoshida, Bromm & Hernquist (2004), see Fang & Cen (2004) for more discussion of constraints on this transition); however a wide range of z redshifts where Pop III stars might be important for reionization have been suggested (between $z = 10$ and $z = 20$ e.g. Wyithe & Padmanabhan (2006), Wyithe & Cen (2006)). (There are even searches for evidence of Pop III stars at redshifts down to $z = 6$ (Scannapieco et al (2006)).) As a result we do not consider redshifts before $z = 12$ (which are active, for our choices of time scales, from mergers at $z = 15$).

There are expected differences at high redshift, for example the higher densities $(1+z)^3$ lead to much shorter cooling times, as well as lower

⁸We choose $f_{\text{esc}} = 0.05$ cf. Wyithe & Loeb (2003)), canonical choices vary by a factor of 10. Loeb et al use $N_{\text{bary}} = 4300$ for a Scalo IMF of metallicity 1/20 of solar.

metallicities, thus these guesses are just that, however they are a starting point for estimating the size of time dependence of \dot{m}_{bh} .

3.2 Black Hole Accretion

We now turn to photon production due to black hole accretion of mass \dot{m} . We take (again assuming a constant photon production rate),

$$\frac{dN_{\text{ph}}^{\text{bh}}}{dt} = \dot{m} c^2 \frac{f_{\text{UV}}}{h\nu_{\text{bh}}} \frac{1}{t_{\text{acc}}} \quad (34)$$

which leads to (using the time dependent version of eqn. 30)

$$t_{\text{ph}}(\dot{m}_i; \dot{m}_0; t_i; \dot{m}; t) = 6.9 \times 10^7 \frac{\dot{m}}{M} \frac{f_{\text{UV}}}{\frac{h\nu_{\text{bh}}}{13.6\text{eV}}} \frac{1}{t_{\text{acc}}} \quad (35)$$

The black hole photon production formula only applies to halos hosting a black hole (i.e. with mass above $m_{\text{bh},\text{min}}(z)$) and includes the effects from UV photons only. The factor $\frac{f_{\text{UV}}}{h\nu_{\text{bh}}} = 0.1 - 0.2 \text{ ryd}^{-1}$ (e.g. Salvaterra, Ferrara & Haardt (2005)). We are assuming that f_{UV} takes into account any local absorption, i.e. it is the flux from the whole region due to the mass accretion. The efficiency is usually taken to be $\epsilon = 0.1$. The mass accreted \dot{m} is often specified in terms of halo mass in the range $10^3 - 10^5 M$. Assuming the mass accretes at the Eddington rate

$$\dot{m}_{\text{bh}} = \dot{m}_{\text{bh}} = \dot{m}_{\text{E}}; \quad \dot{m}_{\text{E}} = 45 M \text{ yr}^{-1} \quad (36)$$

and commonly used black hole mass to halo mass relations, $m_{\text{bh}} = 10^{-3} - 10^{-4} M$, this gives lifetimes t_{acc} from $0.01 - 10 t_{\text{E}}$. We will take a relatively short accretion time, $0.1 t_{\text{E}}$, as our fiducial time t_{acc} .⁹

For our purposes we consider all halos above some minimum mass $m_{\text{bh},\text{min}}(z)$ to host black holes, and all halos below it not to host black holes, and ignore the scatter in this relation. We tried to estimate this minimum mass by using methods already found in the literature. We have two choices corresponding to seed black holes at $z = 24$ in halos which are 3.5 and 3 σ fluctuations, following Madau et al's approach (2004), see the appendix for more discussion of this choice and constraints. The two cases used for minimum halo masses hosting black holes and \dot{m} ($10^4 K$) are shown as a function of redshift in Fig. 1.

⁹Many different concerns suggest a shorter t_{acc} . Relating the black hole mass instead to the halo velocity, $m_{\text{bh}} = 10^{-4} (1+z)^{3-2} M$ i.e. including redshift dependence (Bromley, Somerville & Fabian (2004), Wyithe & Padmanabhan (2006)), lowers t_{acc} . Accretion at super-Eddington rates (argued necessary to get supermassive black holes by redshift 6 or 7, e.g. Haiman (2004)) also gives a shorter t_{acc} . In addition, shorter accretion times are also expected from some low redshift constraints based on the luminosity function (e.g. Wyithe & Padmanabhan (2006)).

3.3 Recipe for Ionizing Photons

Combining the above, we have the following recipe for $\dot{m}_t(m_i; m_0; t_i; m; t)$ due to a m_i halo merging to mass m_0 at time t_i which later ends up in m at time $t < t_i + t_{\text{ion}}$: Besides the merger being within the t_{ion} of inter-

Table 1: "Recipe" for $\dot{m}_t(m_i; m_0; t_i; m; t)$

cause	major merger	\dot{m}_t	t_{ion}
quiescent	{	$\frac{m^{1+}}{\dot{m}_{\text{ref}}^{1+}}$	$t = 80 \text{ M yr}$
starburst	> 1:2.5	$(\dot{m}_{\text{sb}} \dot{m}_{\text{ref}})^{\frac{m_0}{m}} \frac{m^{1+}}{m_{\text{ref}}^{1+}}$	$t_{\text{burst}} + t = 100 \text{ M yr}$
black holes	> 1:10	$\dot{m}_{\text{bh}} m_0$	$t_{\text{acc}} = 0.1 t_S = 4.5 \text{ M yr}$

est (starburst or accretion), the $\dot{m}_t(m_i; m_0; t_i; m; t)$ are also zero unless the masses also satisfy certain conditions. For the mass range cut-off for a major merger we will use 1:2.5 for starbursts (many ranges are used in the literature) and 1:10 for black hole accretion (e.g. Madau et al (2004)). For black holes $m_i > m_{\text{bh}, \text{min}}(z(t_i))$, for quiescent and starburst star formation $m_0 > m_{\text{ax}}(10^4 K(t_i); m_{0, \text{min}}(t_i))$.

Then \dot{m}_{sb} ; \dot{m}_{bh} encapsulate all the non-mass dependent factors:

$$\begin{aligned}
 \dot{m}_{\text{q}} &= f N_{\text{bary}} \frac{f_{\text{esc}}}{t} \frac{1}{X} \\
 &= \frac{.36}{\text{M yr}} \frac{f}{0.1} \frac{N_{\text{bary}}}{4400} \frac{f_{\text{esc}}}{0.05} \frac{80 \text{ M yr}}{t} \\
 \dot{m}_{\text{sb}} &= \frac{1.5}{\text{M yr}} \frac{f_{\text{burst}}}{0.5} \frac{N_{\text{bary}}}{4400} \frac{f_{\text{esc}}}{0.05} \frac{t_{\text{burst}} + t}{0.8} \\
 \dot{m}_{\text{bh}} &= 6.9 \cdot 10^7 \frac{m_0}{t_{\text{acc}} m_0} \frac{f_{\text{UV}}}{\frac{h\nu}{13.7 \text{ eV}}} \frac{m}{h\nu} \\
 &= \frac{15.3}{\text{M yr}} \frac{f_{\text{UV}}}{0.1 \text{ Ryd}} \frac{h\nu}{13.7 \text{ eV}} \left(\frac{m_{\text{bh}}}{10^{-4}} \right) \left(\frac{m}{0.1} \right)
 \end{aligned} \tag{37}$$

Our crucial parameters are shown in the second line of each equation. Our crucial $\beta = 2=3$. The reference mass m_{ref} is taken to change with redshift,

$$m_{\text{ref}}(z) = 4.3 \cdot 10^{10} \left[\frac{m(0)}{m(z)} \frac{\text{crit}(z)}{18^{-2}} \right]^{1=2} \left(\frac{1+z}{10} \right)^{3=2} h^{-1} \text{M} ; \tag{38}$$

(e.g. Wyithe & Loeb (2003)¹⁰). Some numerical studies have found a transition mass m_{ref} which doesn't change significantly with redshift (Keres et al (2005), the corresponding transition mass is also almost a factor of 10 smaller at $z = 0$).

¹⁰They interpret the $m^{2=3}$ behavior as due to a potential well effect. We have taken their default parameter values for $v = 176 \text{ km s}^{-1}$ and $\text{crit} = 18^{-2} + 82x - 39x^2$, $x = \frac{m(z)}{m(0)}$, $m(z) = m(0)(1+z)^3 = [m(0)(1+z)^3 + \dots]$. At $z = 9$, $\text{crit} = 18^{-2} \frac{m(z)}{m(0)}$.

For \dot{m}_{bh} we estimate $\frac{\dot{m}_0}{m_0 t_{acc}}$ assuming an Eddington rate and $\dot{m} = \dot{m}_{bh} < 1$ so that $\dot{m} = \dot{m}_{bh} (e^{t_{acc}=t_s} - 1) \approx \dot{m}_{bh} t_{acc}=t_s$ and we take the black hole mass change proportional to its host halo mass. The suggested relation of black hole mass to halo velocity mentioned earlier would give a larger ratio of black hole mass to halo mass and a bigger effect from black holes. In addition, super Eddington accretion will also shorten t_{acc} and increase \dot{m}_{bh} . Note that changing $t + t_{burst}; t_{acc}$ also changes the range of integration for t_i in calculating \dot{m}_t , not only the prefactors $\dot{m}_{burst}; \dot{m}_{bh}$. For starburst star formation \dot{m}_{burst} gives an effective $\dot{m}_{burst} t = (t + t_{burst})$.

With these assumptions, the $\dot{m}_t(m_i; m_0; t_i; \dot{m}; t)$ in equation 7 are a set of constants, only nonzero when $t_i; m_i; m_0$ are in the right range. All of these numbers rely on a huge number of estimates of unknowns, i.e. the contributions of starbursts, black hole accretion and their relative strengths. As mentioned earlier, ideally one could turn this around and use it to estimate the contributions from starbursts and quasars, but many uncertainties are involved. Here we are interested in the sporadic and time dependent nature of the mergers changing photon production rates.

Using these definitions, $\dot{m}_{ja}(m)$ (equation 7) is shown in Fig. 2 for two black hole assumptions for a series of different times. The black hole and star formation contributions are shown separately as well. The quiescent contributions to \dot{m}_{ja} roughly scale with the dotted line in each case, but do not change with redshift. The ratio of merger-induced photon contributions to total photon contributions for the fiducial model and for the same redshifts is shown in Fig. 3. The source mergers have a similar photon production rate to the quiescent rate, increasing with increasing mass and redshift. There is also a sharp increase in the merger contribution relative to the quiescent contribution once the masses are large enough to host black holes. Although the black holes have a very large contribution per halo for high mass halos, the sharp decline in numbers of halos as mass increases somewhat limits their effects.

4 Consequences for bubbles

The framework and prescriptions of the previous two sections can now be combined to predict the resulting properties of the ionized bubbles. In practice there are two steps: $\dot{m}_t(m_i; m_0; t_i; \dot{m}; t)$ is used to find the required overdensities for given bubble masses M , i.e. $\bar{\rho}_M$. The barriers $\bar{\rho}_M$ then determine the bubble size distributions and the time evolution of the ionization fraction.

Our fiducial model, shown unless otherwise stated, is for the 3:5 seed black holes at $z=24$ as described earlier and in the appendix, with parameters given in eqn. 37. We also considered 3 seed black holes at $z=24$, $\dot{m} = 0$, m_{ref} constant, $f_{esc} = 4f_{esc}$, $\dot{m}_{bh}^2 = 0.0225$, no stars, no black holes, and

cosmological tilt $n = 1.05$. This last model seemed to have very similar effects to the one increasing f_{esc} . We took some combinations of these variations with each other as well. The two lower integration limits for m_0 , ($m_{0\text{min}} = 0.1m$ or $m_{0\text{min}} = m$ ($T = 10^4\text{K}$)) gave very similar results when $\beta = 2=3$. We considered mini halo and MHR recombination for all the models, and MIPS recombination for the fiducial model and 5 representative variations. One other quantity we must fix is an initial condition; this is discussed below.

4.1 Barriers

To find the required \bar{m} given a bubble mass M we use the generalization of equation 3, equation 13:

$$\int_{t_0}^{z_t} dt [(f)_{t_0} A_u (1 + R_{\beta M}(t_0)) \frac{M_{\text{ion}}}{M} C(R_{\text{ion}}(t_0))] = 1 : \quad (39)$$

Because time dependence is built in, we either need to integrate all the way back to the time of the very first ionizing photon production or include some initial condition of global ionization fraction. We choose to fix an initial condition at $z = 12$. At $z = 12$ halos are only active from mergers since $z > 15$ with our choices of relaxation times. As discussed earlier $z = 15$ is the earliest redshift Pop II star dominance (and thus our assumptions) might be expected to hold.

The distribution corresponding to the initial photons is taken to be a time independent (m) of the form given by FMH04 & FMH05, so either F_{MH} is constant or

$$F_{\text{MH}} / f = \begin{cases} (\frac{m}{m_{\text{ref}}})^{2=3} & m < m_{\text{ref}} \\ \text{const} & m > m_{\text{ref}} \end{cases} \quad (40)$$

in accordance with the mass dependence of our τ_t ($\beta = 0;2=3$). Then F_{MH} is normalized by setting the global ionization fraction

$$\int_{m_{\text{min}}}^z dm F_{\text{MH}}(m) P_1(m; \tau_{\text{bc}} M; M) = x_{\text{IBC}} : \quad (41)$$

At a later time, the ions present in a region of mass M with overdensity \bar{m} are a combination of the ions produced in that region at the initial time plus those produced since, minus recombinations:

$$\int_{\tau_{\text{bc}}}^R dm F_{\text{MH}}(m; \tau_{\text{bc}}) P_1(m; \tau_{\text{bc}} M; M) + \int_{\tau_{\text{bc}}}^R dt [(f)_{t_0} A_u (1 + R_{\beta M}(t_0)) \frac{M_{\text{ion}}}{M} C(R_{\text{ion}}(t_0))] = 1 : \quad (42)$$

For our fiducial model, we start with an ionization fraction $x_1(z = 12)$ of almost zero (10^{-3}). This should isolate the evolution of bubble properties due to the change in photon production since the initial time. We also experimented with some non-negligible initial photon distributions at $z = 12$

($x_i = 10^{-2}; 10^{-1}; 0.5; 0.14$) and an initial condition of $x_i = 10^{-3}$ at $z = 16$ when halos are active from mergers since $z = 23$. This last corresponded to $x_i = 0.14$ at $z = 12$. In practice at $z = 16$ Pop II stars are much less likely and our assumptions about photon production rates suspect, as a result this model was not our fiducial model, but is useful for studying effects of initial conditions.

To find $R_{\text{ion}}(t)$ the integral is divided into 700 steps from the initial time to the redshift of interest. At each time, the instantaneous change in ionized mass fraction (df_{ion}/dt) is added to the mass fraction already present (the integral up to that time) to find M_{ion}/M , the ionized mass fraction. In the case where more photons were produced than hydrogen atoms in the region, we took $M_{\text{ion}}/M = 1$ (allowing it greater than one had a negligible effect). We took $R_{\text{ion}} = \left[\frac{M_{\text{ion}}}{\frac{4}{3}(1 + R_{\text{M}}(t))} \right]^{1/3}$, however replacing $\frac{3M_{\text{ion}}}{4} \rightarrow M_{\text{ion}}$ or even $\frac{3M}{4}$ had very small effects. The biggest effect of considering reionizations only of M_{ion} are due to the overall coefficient $\frac{M_{\text{ion}}}{M}$. Larger numbers of steps gave indistinguishable results.

We show in Fig. 4 examples of the resulting barriers \bar{r}_M at $z = 7, 8, 9, 10, 11$ and 11.9 for our fiducial model and the three recombination prescriptions. At large radius, $C_{\text{MHR}}(R)$ tends to approach a constant, C_{MIPS} is constant, and $C_{\text{minihalo}}(R)$ increases exponentially. Thus the barriers for minihalo recombination are cut off at large radius. MIPS and MHR recombinations allow bubbles to get very large, if there is sufficient photon production, to the point where consistency questions involving e.g. travel times within the corresponding bubbles arise. For plots of many of the models we thus choose to only include the cases with radii $< 100 h^{-1} \text{Mpc}$, models with much larger radii do appear but are difficult to interpret.

Our time dependent approach produces results which interpolate between the two limits used in earlier works (e.g. FZH04, FO05, FMH05): they included implicit recombinations at early times, and imposed equilibrium between instantaneous photon production and recombination rates at late times. For small bubbles, the photon mean free path exceeds the bubble radius, thus photons escape freely and recombinations do not play an important role; this is expected to happen at early times. As bubbles grow in size, the barriers for ionized regions decrease as a function of bubble radii, since more and more mass (and therefore ionizing photons) can be included in the region. At late times, bubble radii grow to exceed the photon mean free paths and recombinations limit the growth of bubbles. Of the three assumed IGM gas density distributions, the minihalo and MIPS models put more stringent constraints on the bubble growth than the MHR model. The stronger effects of minihalo recombination compared to MHR recombination were also observed in the models equating instantaneous recombination and photon production (FMH05 and FO05).

4.2 Bubble Size Distribution

The barriers found as a function of bubble radii translate directly into mass weighted ionized mass fraction distributions $M^{-2}n_b(M; M)$ as a function of radii, the maximum mass M_c corresponds to a characteristic radius $R_c = [3M_c = (4 - (1 + R_{M_c}(t)))^{1-3}]$ (e.g. FMH05). Descriptions of how to derive the resulting bubble mass function $n_b(M; M)$ for linear barriers can be found e.g. in Sheth & Tormen (1998) and McQuinn et al (2005a). As the barriers here are non-linear in M , we find $n_b(M; M)$ by simulating 4000 random walks directly for each $(M; M)$ combinations. For linear barriers, 4000 steps reproduced the ionization fractions to a 5-10% percent once $x_i > 0.01$. In Fig. 5, we show R vs. $M^{-2}n_b(M; M)$ for the sequence of different redshift barriers of Fig. 4 above. The trends shown here were seen in our other models as well. For all the models, the radii and mass weighted ionized mass fraction grow with time.

For minihalb recombinations the width of the probability distribution for R narrows as R increases and the universe ages. This schematically shows the progress of reionization: at early times bubbles are small and have a large range in sizes, depending more strongly on the local density and ionizing photon production where the bubbles live. As the global ionization fraction grows, or as the bubble volume filling factor increases, bubbles grow in size, slowed by recombinations. Finally bubbles saturate in radii and have similar sizes. In this scenario we expect to find small bubbles with a large scatter in size during early reionization, and large bubbles with similar sizes at late reionization. The narrowing of bubble width with increased ionization fraction was also seen in the studies of limiting cases in earlier work.

For MHR recombinations, the bubble distributions do not narrow at late times, instead recombinations are so weak that the bubble sizes tend to have runaway behavior, getting larger and spreading more as reionization proceeds. MIPS recombinations are seen here to limit the growth of bubble regions, however in models where more photons are produced the radial distribution moves to large R as is seen in the MHR case above for late times (large x_i).

4.3 Ionization Fraction

The global ionization fraction is the fraction of mass inside bubbles at any given time; time histories are shown in Fig. 6 for the MHR, minihalb and MIPS recombination ansatzes with the crucial photon production model. Even with negligible photons present initially, the ionization fraction gets close to 1 by $z = 7$ for minihalb and MHR recombinations. For comparison, a model of FMH05 is also shown (given by equation 40). At early times the ionization fraction grows more slowly for this time independent model as

the mergers increase photon production as a function of mass more steeply than the $m^{2=3}$ slope. At late times recombinations become more important in the full models and slow reionization, hence, relative to them x_i for the FMH05 model increases more quickly. The cases for stars only and 3.5 black holes only are shown as well.

4.4 Scatter: model variations

There is scatter in the results both from model-to-model variations and to the merger-induced scatter within one model. In order to see similarities and variations between models, we show four different comparisons in Fig. 7. The two top plots show the effects of the $z = 12$ initial conditions on the mass weighted ionized mass fraction for different redshifts. The curves are for the fiducial $x_i(z = 12) = 10^{-3}$ model and $x_i(z = 12) = 10^{-2}; 10^{-1}$: At right we show the fiducial model and $x_i(z = 12) = 0.5$. By $z = 10$ all the models with x_i at $z = 12 = 0.1$ predicted close to identical bubble radii distributions. The model with $x_i = 0.5$ at $z = 12$ has the radii and ionization fraction changing much more slowly between $z = 12$ and $z = 9$, and then converging to the other cases. In addition, the $x_i(z = 16) = 10^{-3}$ and $x_i(z = 12) = 0.14$ models (not shown) gave extremely similar radial distributions at redshifts 7, 8, 9, 10, 11, 11.9. The bottom two plots consider a sampling of different models: different redshifts, photon production rates, recombinations, cosmologies, etc. At lower left models with similar x_i but otherwise widely varying assumptions are shown. A variety of models give very similar shapes, but there is a large scatter (here seen for $x_i = 0.91$, the peaks further to the right correspond to MHR recombinations). The characteristic radius R_c for several hundreds of our model variants is shown at lower right, the general trend of larger radii corresponding to larger ionization fraction is clearly visible, with a spread that can be read off of the plot.

4.5 Scatter: merger induced for a fixed model

The scatter in the photon production rates for a given model due to mergers was described in 2.4. To propagate the scatter in photon production rates calculated from Eq. (29) to the scatter in bubble barriers, we replace

$$\frac{d}{dt} (f)_t \rightarrow \frac{d}{dt} (f)_t + \frac{\sigma}{z} \frac{d}{dt} (f)_t \quad (43)$$

in Eq. (42). We add the scatter of the initial condition $(\frac{\sigma}{z})_{ic}$, corresponding to the first term in equation 42) in quadrature to $(\frac{d}{dt} (f)_t)^2$. We take this initial condition scatter to also be Poisson in accord with our assumption (and that of FMH05) that the initial condition sources are Poisson distributed in the bubbles. The resulting barriers (overdensities) are those required for a

region of mass M to be ionized if the sources within have the one-sigma fluctuation calculated above.

The corresponding barriers for the fiducial model are shown at $z = 10$ in Fig. 8, for all three recombination models. The central line indicates the average barrier $\bar{\mu}_M$, while the higher (lower) barrier μ_M corresponds to the smaller (larger) photon production rate of one-sigma fluctuations in $(f)_t$. At small bubble radii, the scatters around the mean values are large, while at large radii, the three barriers converge to the limiting bubble radius. Smaller bubbles presumably contain fewer halos, so the scatter of photon rates per source plays a relatively important role in determining the required overdensity for bubbles; conversely, larger bubbles contain more halos and thus the effects of the scatter average out within. This trend was seen in all the cases we studied. Producing fewer photons can lead to a scatter up or down in bubble radius: fewer photons means fewer ions all around, but the bubbles present are often required to be larger in order to enclose a sufficient number of sources. As in the case without scatter, for low R_{MHR} and m_{inhalo} recombinations are relatively weak and thus give similar results.

The corresponding radii distributions for these barriers are shown at top left and right and bottom left in Fig. 9. At bottom right the scatter is shown for the m_{inhalo} case for the model with $x_i = 10^{-3}$ at $z = 16$, for the corresponding fiducial model with $x_i = 0.14$ at $z = 12$ and for this fiducial model with the scatter doubled. The scatter for the model evolved from $z = 16$ is much larger: mergers increase the scatter significantly when included over a longer period of time (however recall starting at $z = 16$ with Pop II stars isn't expected to be realistic, this example serves only to illustrate that the initial conditions and time play a large role in the scatter).

The full mass weighted ionized mass fraction distribution is found by combining the scattered barriers and the mean one in a distribution, with some weighting. In principle there is a sequence of barriers corresponding to adding and subtracting the fluctuations with a continuous coefficient rather than just the two cases above, with larger coefficients having smaller weights in the joint distribution. Each random walk used to find the mass weighted ionized mass fraction then has a different barrier ("walk barrier") sampled from this distribution of barriers. At large scales all the walk barriers coincide, but at smaller scales fluctuations between different possible barriers come into play to give a range of walk barriers. The first crossings of each walk barrier are dependent both on the shapes of the barriers in the distribution and on the scales at which each barrier appears. A fluctuation from a higher barrier down to a lower barrier in a walk barrier at some mass M will produce first crossings not only of a path which was counted in the mass weighted ionized mass fractions shown above, but also of any path which would have had first crossings earlier for this lower barrier but didn't for the higher barrier. If there was only one such transition between the barriers

above and it was at a fixed M for all walk barriers, there would be a large spike at the mass scale of the transition, due to all these paths being included at the same M . (Likewise a drop would be expected for a sole transition from a low barrier to a high barrier in a walk barrier.) We do not expect these extreme cases to occur for many walk barriers however, and the transition masses M will change as well. Most of the time the walk barrier will sample the different barriers often enough that a "pileup" of paths that would have crossed earlier, causing such a spike, should be suppressed, similarly for the sharp signal associated with a single jump up to a higher barrier. In general, we expect each walk barrier to sample our 3 barriers frequently, and effects from different walk barriers (different samplings of the barrier distribution) to average out, so that the resulting mass weighted ionized mass fraction distribution becomes close to a weighted average of the corresponding distributions for the 3 barriers shown above.

Some general trends were seen across many models and redshifts. The scatter effects for the families of models are summarized in Fig. 10 (as mentioned above MHR and MIPS cases with $R_c > 100h^{-1} \text{ Mpc}$ are left out but models with $\beta = 0$ are included). The total scatter seems small in all other cases and the radii converge to a value independent of initial conditions (but dependent upon each model's photon production rates). We call the peak of the distributions in R (such as above) for the scattered model R_{scat} and the peak for the fiducial model R_{ave} in these plots. The scatter decreases with increasing radius and decreasing redshift. This is shown in the upper and lower left plots: the upper left plot shows the effect of reduced scatter with increasing numbers of sources (R) included as mentioned earlier, at lower left is the redshift dependence. The ratio $R_{\text{scat}}/R_{\text{ave}}$ also decreases as a function of increased ionization fraction x_i , shown at upper right. At lower right it is shown that the model-to-model scatter is often larger than the merger-induced scatter. The average curves for $M^2 n_b(M; M)$ are shown for a series of models at $z = 9$ along with the representative scattered curves for one of them. Note that the mass ratios chosen to define a major merger will also affect the scatter, for example relaxing the major merger mass ratio leads to more mergers overall and thus smaller Poisson fluctuations.

4.6 Bubble Boundaries

One interesting question is how the ionization fraction decreases from 100% as one goes outside a fully ionized bubble at any given time (we thank Evan Scannapieco for suggesting this calculation and Steve Furlanetto for discussions about its interpretation). If the ionization fraction dropped from fully ionized to e.g. 90% ionized very slowly in space, or if bubbles were very close and connected by high density bridges, relaxing the constraint from fully ionized to 90% ionized would give a very different distribution of barriers and

corresponding radii. To calculate the 90% ionized case we relax the complete ionization requirement for bubbles to

$$\int_{t_{bc}}^R dm_{FMH}(m; t_{bc}) P_1(m; t_{bc}; M; M) + \int_{t_{bc}}^t dt^0 [(f)_{t^0} A_u (1 + R_M(t^0))^{\frac{M_{ion}}{M}} C(R_{ion}(t^0))] = 0.9 : \quad (44)$$

The bubble radii, for minihal and MHR recombinations, are compared for 90% ionized and 100% ionized bubbles in Fig. 11. From Fig. 11 it is seen that these would-be bubbles tend to have very similar sizes compared to completely ionized bubbles. The main exception is when the global ionization fraction is close to one for MHR recombination, perhaps indicating that a significant amount of bubble merging is occurring and/or that there are large regions near the bubbles (perhaps not in 100% ionized bubbles) with high average ionization fraction. For the above models and a sample of others, the fraction of mass 90% ionized or more is within 6% of the mass in regions which are fully ionized at $z = 7$, the difference increases to $< 15\%$ at $z = 11$.

5 Conclusions

We have calculated, via a microscopic model, contributions to $t_{ra}(m)$ including mergers, a time and mass dependent phenomena. Using three recombination histories and several different parameterizations of the uncertain microphysics, the requirements for bubble formation, characteristic radii and ionization fraction histories were then found. The requirements for bubble formation (M) interpolate between the two limits considered in previous work, as expected. The increased photon production due to mergers gives a faster rise in ionization fraction at early times, and then a slower one as recombinations become important. The width of the distribution for the bubble radii narrows for minihal recombinations at later times just as found in earlier work on instantaneous and time independent models. The scatter is largest for bubbles with small numbers of sources, and the model-to-model scatter tends to be larger than the merger induced scatter within a model.

The formalism and tools developed here and results found can be extended in future work. Many other parameter choices also fall well within the range of reasonable guesses due to the large uncertainties at early times, explorations of these would be very interesting. Pop III stars can be included in the same framework as well. The observational consequences of the trends we have identified in our models so far are also a clear next step. This can be done using analytic methods based on the distributions we have found. Another route would be to implement the t merger prescriptions into numerical simulations of histories or semi-analytic simulations such as those of Zahn et al (2006), and calculate the observational consequences this way.

Our methods might also be important for other descriptions of reionization, e.g. due to the clustering of galaxies such as is described in Babich & Loeb (2005).

We both thank the Aspen Center for Physics and the January winter meeting organizers for the opportunity to present this work when it was near completion. We are grateful to many people for helpful suggestions, pointers to literature and explanations, including A. Barth, M. Boylan-Kolchin, D. Eisenstein, J. Greene, J. Hennawi, G. Howes, I. Iliev, D. Keres, M. Kuhlen, C. P. Ma, A. Meiksin, C. McKee, M. Morales, P. Norberg, E. Quataert, B. Robertson, E. Scannapieco, R. Sheth, F. van den Bosch, A. Wetzel and O. Zahn. We want to thank S. Furlanetto in particular for numerous explanations and discussions and comments on the draft. Last but not least, JDC thanks M. White for more discussions about this topic than he ever wanted to have. JDC was supported in part by NSF-AST-0205935 and T.C. Chang was supported in part by NSF as well.

Appendices

Extended Press-Schechter definitions

Two probabilities appear in our formalism in the text. The probability that a halo of mass m at time t contains a halo of mass m_0 at time t_i is:

$$P_1(m_0; t_i | m; t) dm_0 = \frac{1}{2} \frac{d^2(m_0)}{dm_0} \left[\frac{c(t_i)}{c(t)} \frac{c(t)}{c(t_i)} \right]^{3=2} \exp \left[-\frac{(c(t_i)/c(t))^2}{2} \frac{c(t)}{c(t_i)} \right] g dm_0 \quad (45)$$

The overdensity for collapse at time t_i is taken to be time dependent, $c(t_i) = 1.68 D(z_i)$ where $D(z_i)$ is the growth factor, and $\sigma_i^2 = (m_i)^2$ and $\sigma^2 = (m_0)^2$, the variance of the linear power spectrum smoothed over a region of mass m (at $z=0$). The factor of $m_0 = m_i$ converts from the number of points in such halos to the number of such halos.

The other quantity is the time derivative of the above, the fraction of halos that have mass m_0 that have jumped at time t_i from mass m_i :

$$P_1(m_i \rightarrow m_0; t_i) \frac{m_0}{m_i} dm_i dt_i = \frac{1}{2} \frac{1}{(\sigma_i^2)^{3=2}} \left[\frac{d c(t_i)}{dt_i} \right] \frac{d^2 m_0}{dm_i m_i} dm_i dt_i : \quad (46)$$

Minimum black hole masses

We describe here how we chose our minimum host halo masses for harboring black holes. For $m_{bh, min}(z)$ many suggestions of high redshift black hole histories are available, see for example the review by Haian & Quataert

(2004) and references therein. We take our black holes to be descendants of the very first stars, expected to be extremely massive due to the difficulty of fragmentation (see for example Bromm, Coppi & Larson (1999; 2002), Nakamura & Umemura (1999; 2001), Abel, Bryan & Norman (2000; 2002), Schneider et al (2002)). At the end of the lifetimes of these stars, very massive black holes are expected to form, e.g. Madau & Rees (2001), however the initial mass distribution of the stars and their resulting black holes are unknown (many different examples are considered in e.g. Alvarez, Bromm & Shapiro (2006), O'Shea et al (2005), Scannapieco et al (2006), and Madau et al (2004)).

We follow Madau et al (2004) and consider two cases, putting very massive black holes in all > 3 or > 3.5 fluctuations at redshift $z = 24$, corresponding to masses m_3 ; $m_{3.5}$ ($m > 1.4 \cdot 10^5 h^{-1} M_\odot$; $m > 1.4 \cdot 10^6 h^{-1} M_\odot$) which then grow primarily through mergers. We find the minimum mass for black holes at our (later) time of interest by requiring at least 90% of the halos with mass $m_{bh, min}(z)$ to have at least one halo of mass $m_{bh, min}(z = 24)$ in it, using extended Press-Schechter. (In practice it appears that at least 4 or 5 mergers occur for these high peaks by $z = 15$, we thus require at least the corresponding number of paths originally at mass m_1 to be present in each final mass halo of mass m at time t in order for that mass to host a black hole. We assume the black holes merge when their halos do, e.g. Mayer et al (2006), there is still discussion on this issue, see e.g. Madau et al (2004) for further discussion including considerations of black hole ejection.) A second option for estimating halo masses which can contain seed black holes is using the requirement of low angular momentum disks which can collapse, the two reference models for minimum black hole mass used by Koushiappas, Bullock & Dekel (2004) at $z = 9; 12; 15$ are approximately the same as those we find extrapolating the minimum mass halos of Madau et al (2004) for 3 and 3.5 host halos at $z = 24$. (For some reason Madau et al (2004) get a much lower merger rate than we do, ours is more in accord with the calculations of Koushiappas et al (2004).) As we are interested in some reasonable black hole mass estimates, the similarity between these two calculations suggests these are useful reference masses to consider. This is certainly not the only way to estimate the black hole host masses, other options include tracing the luminosity function back in time e.g. Wyithe & Loeb (2002).

Black hole radiation in principle constrains black hole masses and numbers. However, compounding the the black hole/host halo mass relation uncertainties and accretion mode/speed uncertainties mentioned earlier are even more uncertainties tied to black hole radiation estimates. Harder X-ray photons may induce additional ionizations (some estimates have X-rays dominate the luminosity, e.g. Madau et al (2004)) in regions with low ionization fractions, in addition, efficiencies might be higher (Haiman & Quataert (2004)). The strongest direct constraints on early black holes is that they

don't produce photons that exceed the unresolved soft X-ray background (Dijkstra, Haiman & Loeb (2004), Salvaterra, Ferrara & Haardt (2005)). This translates into a constraint on the ratio of power law to multicolor disk luminosities; although we use Madau et al's (2004) original model of including black holes we take $\alpha < 1$ to avoid the constraints their models could not satisfy ($\alpha = 0.1$ is common today). Other black hole halo mass constraints requiring more evolutionary assumptions over longer periods of time include predicting correctly black hole to halo mass ratios today (e.g. Ferrarese & Merritt (2000)), the number of intermediate mass black holes today (Yu & Tremaine (2002)) and the observed quasar activity observed up to $z = 6$. In addition, one expects starbursts and black hole growth can be related using the relation between central black hole mass and bulge velocity dispersion¹¹, models proposed to do this explicitly include those by Cattaneo et al (2005) and Enoki et al (2003).

Other scatter assumptions

Other assumptions are possible for

$$\ln(m; t; M; M) \ln(m^0; t^0; M; M) \quad (47)$$

and

$$\ln^a(m; t; M; M) \ln^b(m^0; t^0; M; M) \quad (48)$$

besides those used in the main body of this paper. We list two more possibilities for each.

For $\ln(m; t; M; M) \ln(m^0; t^0; M; M)$, one might expect that a large fluctuation at time t implies a large fluctuation at time $t^0 = t + \tau$, giving a correlation between different $t; t^0$. In addition, halos of mass m at time t will have a different mass m^0 at time t^0 , so the fluctuations will be related for $m \notin m^0$ and $t \notin t^0$.

One possibility is to give the scatter a decay time (or characteristic τ_{rel}) and a decay mass m_{rel} ,

$$\ln(m; t; M; M) \ln(m^0; t^0; M; M) = e^{-(t^0 - t)/\tau_{rel}} e^{-(m - m^0)/m_{rel}} \ln(m; t) \quad (49)$$

Other possibilities are to have the decay depend on t rather than (t) and m rather than m^0 .

Another possibility is to say that the relation between the mean values of $\ln(m; t; M; M)$ and $\ln(m^0; t^0; M; M)$

$$\begin{aligned} \ln(m; t; M; M) \ln(m^0; t^0; M; M) = \\ \int_{m^0 < m; t^0 < t} \ln(m; t; M; M) \ln(m^0; t^0; M; M) \frac{m}{m^0} n(m; t; M; M) \quad (50) \end{aligned}$$

¹¹We thank Joe Hennawi for this suggestion.

suggests a relation between the scatters for $m^0 < m; t^0 < t$ as follows:

$$\begin{aligned} \ln (m ; t; M ; M) n (m^0 ; t^0; M ; M) i &= \ln (m ; t; M ; M) \int_{m^0}^m \int_{t^0}^t P_1 (m^0 ; t^0; jn^0 ; t) \frac{m}{m^0} n (m ; t; jn ; t) i \\ &= n (m ; t; M ; M) n (m^0 ; t^0; M ; M) \\ &+ \frac{1}{V_M} (t - t^0) \int_{m^0}^m \int_{t^0}^t P_1 (m^0 ; t^0; jn^0 ; t) (m - m^0) n (m ; t; M ; M) \\ &= n (m ; t; M ; M) n (m^0 ; t^0; M ; M) \\ &+ \frac{1}{V_M} (t - t^0) \frac{m}{m^0} P_1 (m^0 ; t^0; jn ; t) n (m ; t; M ; M) ; \\ m^0 < m ; t^0 < t : \end{aligned} \tag{51}$$

and similarly when $(m ; t) \geq (m^0 ; t^0)$ when $m^0 > m ; t^0 > t$. This is not required: the relation between the average values does not have to be followed by the scatter, it is an additional modeling assumption.

The equal mass and time limit, $m \rightarrow m^0 ; t \rightarrow t^0$ can be taken in the above. Writing $x = m - m^0$ and $y = t - t^0$ we have

$$P_1 (x ; y) = \frac{1}{2} \frac{y}{x^{3/2}} e^{-y^2/(2x)} \frac{dx}{dm} = \frac{d}{dy} \left[\frac{1}{2} \frac{1}{x^{1/2}} e^{-y^2/(2x)} \right] \frac{dx}{dm} ; \tag{52}$$

then $m \rightarrow m^0$ is $x \rightarrow 0$ and $t \rightarrow t^0$ is $y \rightarrow 0$. The two limits do not commute, thus another assumption is involved, we take $m \rightarrow m^0$ first, roughly writing $\int_{m^0}^m dm = \int_{m^0}^m (m - m^0) + (m^0 - m) + (D(m - m^0) - 1)$ and then recognize the Dirac delta function as the $x \rightarrow 0$ limit of the quantity in square brackets. This also assumes taking this limit and taking the derivative commute. We then get the full two point function for these assumptions to be:

$$\begin{aligned} \ln (m ; t; M ; M) n (m^0 ; t^0; M ; M) i &= n (m ; t; M ; M) n (m^0 ; t^0; M ; M) \\ &+ \frac{1}{V_M} (t - t^0) \frac{m}{m^0} P_1 (m^0 ; t^0; jn ; t) n (m ; t; M ; M) \\ &+ \frac{1}{V_M} (t^0 - t) \frac{m}{m^0} P_1 (m ; t; jn^0 ; t^0) n (m^0 ; t^0; M ; M) \\ &+ \frac{1}{V_M} (m - m^0) D (t - t^0) n (m^0 ; t^0; M ; M) \end{aligned} \tag{53}$$

The derivative of $D(y)$ is evaluated by integrating by parts and changing variables to $t; t^0$.

There is also a range of possibilities for the scatter in $t_a(m)$ or $n^a(m^0; jn; t)$. Again, we describe two.

One possibility is to take the same scatter as is used for $n(m; t; M; M)$ and use it for $P_1(m^0; t; jn; t) = \frac{m^0}{m} n(m^0; t; jn; t)$ and then define the scatter for $P_1(m; t; jn; t)$ as the limit. Naive attempts to take this limit give a divergence however.

One also might say that a halo of mass m_0 in a halo of mass m has either had or not had a recent merger, which suggests a binomial distribution, and that if the total number of halos of mass m_0 in $m; t$ halos is N that this number is then pN , implying a scatter $Np - p^2N$ rather than the poisson Np . Implementing this appears to require yet another assumption because the time integral of the rate appears, but it will decrease the scatter from Poisson (Np).

None of these scatter prescriptions is required given current knowledge, thus in the main body of the text we used the simplest version. It is reasonable to expect that the trends of largest scatter for smallest radii will continue as large numbers of enclosed halos will tend to enclose the mean number of mergers.

References

- [2000] Abel, T., Bryan, G., Norman, M. L., 2000, *ApJ* 540, 29
- [2002] Abel, T., Bryan, G., Norman, M. L., 2002, *Science*, 295, 93
- [2006] Alvarez, M. A., Bromm, V., Shapiro, P. R., 2006, *ApJ* 639, 621
- [2005] Alvarez, M. A., Komatsu, E., Dore, O., Shapiro, P. R., 2005, *astro-ph/0512010*
- [2001] A. Andreu, G. Gonzalez-Casado, E. Salvador-Sole, 2001, *MNRAS* 327, 939
- [1972] Arons, J., Wingert, D. W., 1972, *ApJ* 177, 1
- [2005] Babich, D., Loeb, A., 2005, *astro-ph/0509784*
- [2006] Bagla, J. S., Prasad, J., 2006, *astro-ph/0601320*
- [2001] Becker, R. H., et al, 2001, *AJ* 122, 2850
- [1991] Bond, J. R., Cole, S., Efsthathiou, G., Kaiser, N., 1991, *ApJ* 379, 440
- [2001] Barkana, R., Loeb, A., 2001, *PhR* 349, 125
- [2004a] Barkana, R., Loeb, A., 2004, *ApJ* 609, 474
- [2005] Barkana, R., Loeb, A., 2005, *astro-ph/0510421*
- [2005] Benson, A. J., Kamionkowski, M., Hassani, S. H., 2005, *MNRAS*, 357, 847
- [1991] Bower, R., J., 1991, *MNRAS*, 248, 332
- [2004] Bromley, I. M., Somerville, R. S., Fabian, A. C., 2004, *MNRAS*, 450, 356
- [1999] Bromm, V., Coppi, P. S., Larson, R. B., 1999, *ApJ*, 527, L5
- [2002] Bromm, V., Coppi, P. S., Larson, R. B., 2002, *ApJ*, 564, 23

- [2002] Casas-Miranda, R., Mo, H. J., Sheth, R. K., & Boemer, G., 2002, *MNRAS* 333, 730
- [2005] Cattaneo, A., Blaizot, J., Devriendt, J., Guiderdoni, B., 2005, *MNRAS* 364, 407
- [2000] Cavaliere, A., Vittorini, V., 2000, *ApJ*, 543, 599
- [2003] Ciardi, B., Stoehr, F., White, S. D. M., 2003, *MNRAS*, 343, 1101
- [2006] Ciardi, B., Scannapieco, E., Stoehr, F., Ferrara, A., Iliev, I. T., Shapiro, P. R., 2006, *MNRAS* 366, 689
- [2006] Conselice, C. J., 2006, *ApJ* 638, 686
- [2006] Cooray, A., Barton, E., eds., 2005, "First Light and Reionization: Theoretical Study and Experimental Detection of the First Luminous Sources", *New AR* 50
- [2006] Dave, R., 2006, *New AR* 50, 24
- [2004] Dijkstra, M., Haiman, Z., Loeb, A., 2004, *ApJ* 613, 646
- [1997] Eisenstein, D., Hu, W., 1997, *Apj* 511, 5
- [2003] Enoki, M., Nagashima, M., Gouda, N., 2003, *Publications of the Astronomical Society of Japan*, 55, 133
- [2003] Fan, X., et al 2003, *AJ*, 125, 1649
- [2006] Fan, X., Carilli, C. L., Keating, B., 2006, astro-ph/0602375, *ARA & A* to appear.
- [2004] Fang, T., Cen, R., 2004, *ApJL* 616, 87.
- [2000] Ferrarese, L., Merritt, D., 2000, *ApJ* 539, 9L
- [2004] Furlanetto, S. R., Briggs, F. H., 2004, *New Astronomy Review*, 48, 1039
- [2004] Furlanetto, S. R., Hemquist, L., Zaldariagga, 2004, *MNRAS*, 354, 695
- [2004a] Furlanetto, S. R., Zaldariagga, M., Hemquist, L., 2004, *ApJ* 613, 1
- [2004b] Furlanetto, S. R., Zaldariagga, M., Hemquist, L., 2004, *ApJ* 613, 16
- [2006] Furlanetto, S. R., Zaldariagga, M., Hemquist, L., 2006, *MNRAS*, 365, 1012

- [2005] Furlanetto, S.R., Quinn, M., Hemquist, L., 2005, 2006, *MNRAS* 365, 15
- [2005] Furlanetto, S.R., Oh, S.P., 2005, *MNRAS* 363, 103
- [2001] Jang-Condell, H., Hemquist, L., 2001, *ApJ* 548, 68
- [2000] Gnedin, N.Y., 2000, *ApJ* 535, 530
- [2004] Haiman, Z., 2004, *ApJ*, 613, 36
- [2004] Haiman, Z., Quataert, E., 2004, in *Supermassive Black Holes in the Distant Universe*, Ed. A. J. Barger, Kluwer Academic Publisher, Dordrecht.
- [2006] Heitmann, K., Lukic, Z., Habib, S., Ricker, P.M., 2006, [astro-ph/0601233](https://arxiv.org/abs/astro-ph/0601233)
- [2005] Iliev, I.T., Scannapieco, E., Shapiro, P.R., 2005, *ApJ* 624, 491
- [2005] Iliev, I.T., et al., 2005, *MNRAS* 361, 405
- [2006] Mellem, G., Iliev, I.T., Pen, U.-L., Shapiro, P.R., 2006, in prep.
- [2000] Kauffmann, G., Haehnelt, M., 2000, *MNRAS* 311, 576
- [2003] Kauffmann, G., et al., 2003, *MNRAS* 341, 54.
- [2005] Keres, D., et al., 2005, *MNRAS* 363, 2
- [1996] Kitayama, T. & Suto, Y., 1996, *MNRAS* 280, 638
- [2005] Kohler, K., Gnedin, N.Y., Hamilton, A.J.S., 2005, [astro-ph/0511627](https://arxiv.org/abs/astro-ph/0511627)
- [2004] Koushiappas, S.M., Bullock, J.S., Dekel, A., 2004, *MNRAS*, 354, 292
- [1993] Lacey, C., Cole, S., 1993, *MNRAS*, 262, 627
- [1994] Lacey, C., Cole, S., 1994, *MNRAS*, 271, 676
- [2001] Loeb, A. & Barkana, R., 2001, *ARA & A*, 39, 19
- [2005] Loeb, A., Barkana, R., Hemquist, L., 2005, *ApJ* 620, 553
- [2006] Loeb, A., 2006, to be published by Springer, [astro-ph/0603360](https://arxiv.org/abs/astro-ph/0603360)
- [2003] Machacek, M.M., Bryan, G.L., Abel, T., 2003, *MNRAS*, 338, 273
- [2001] Madau, P., Rees, M.J., 2001, *ApJ*, 551, L27

- [2004] Madau, P., Rees, M. J., Volonteri, M., Haardt, F., Oh, S. P., 2004, *ApJ* 604, 484
- [2006] Mayer, L., et al, 2006, *astro-ph/0602029*
- [2005a] McQuinn, M., Furlanetto, S. R., Hemquist, L., Zahn, O., Zaldarriaga, M., 2005, *ApJ* 630, 643
- [2005b] McQuinn, M., Zahn, O., Zaldarriaga, M., Hemquist, L., Furlanetto, S., 2005, *NewAR* 50, 84
- [1994] Mihos, J., Hemquist, L., 1994, *ApJ*, 425, 13
- [1996] Mihos, J., Hemquist, L., 1996, *ApJ*, 464, 641
- [2000] Miralda-Escude, J., Haehnelt, M., & Rees, M. J., 2000, *ApJ* 531, 1
- [2002] Mo, H. J., White, S. D. M., 2002, *MNRAS* 336, 112
- [1999] Nakamura, F., Umemura, M., 1999, *ApJ*, 515, 239
- [2001] Nakamura, F., Umemura, M., 2001, *ApJ*, 548, 19
- [2005] Naoz, S., Barkana, R., 2005, *MNRAS* 362, 1047
- [2005] Oh, S. P., Furlanetto, S., 2005, *ApJL* 620, 9
- [2005] O'Shea, B. W., Abel, T., Wahlen, D., Norman, M. L., *ApJ* 628, L5
- [2001] Papovich, C., Dickinson, M., Ferguson, H. C., 2001, *ApJ*, 559, 620
- [1974] Press, W., Schechter, P., 1974, *ApJ* 187, 425
- [1998] A. Raig, G. Gonzalez-Casado, E. Salvador-Sole, 1998, *ApJ* 508, L129
- [2002] Razoumov, A. O., et al, 2002, *ApJ* 572, 695
- [2003] Reed, D., et al, 2003, *MNRAS* 346, 565
- [2005] Reed, D., et al, 2005, *MNRAS* 363, 393
- [1998] E. Salvador-Sole, J.S. Solanes, A. Manrique, 1998, *ApJ* 499, 542
- [2005] Salvaterra, R., Haardt, F., Ferrara, A., 2005, *astro-ph/0507208*, *MNRAS* in press
- [2006] Scannapieco, E., et al, 2006, *NewAR* 50, 89
- [2002] Schneider, R., Ferrara, A., Nataraajan, P., Omukai, K., 2002, *ApJ* 571, 20

- [2005] Shapiro, P. R., et al, 2005, astro-ph/0512516
- [2001] Shapley, A., et al., 2001, ApJ, 562, 95
- [1998] Sheth, R., et al., 1998, MNRAS 300, 1057
- [1999] Sheth, R., Lemson, G., et al., 1999, 304, 767
- [2002] Sheth, R., Toomey, G., et al., 2002, MNRAS 329, 61
- [2003] Sokasian, A., Abel, T., Hernquist, L., Springel, V., et al., 2003, MNRAS, 344, 607
- [2004] Sokasian, A., Yoshida, N., Abel, T., Hernquist, L., Springel, V., et al., 2004, MNRAS 350, 47
- [2003] Somerville, R. S. & Livio, M., et al., 2003, ApJ 593, 611
- [2006] Spergel, D. N. et al, 2006, to appear
- [2005] Springel, V., Di Matteo, T., Hernquist, L., et al., 2005, MNRAS 361, 776
- [2005] Warren, M. S., Abazajian, K., Holz, D. E., Teodoro, L., et al., 2005, astro-ph/0506395
- [2004] White, R. L., et al, 2004, AJ 126, 1
- [2005] White, R. L., et al, 2005, AJ 129, 2102
- [2002] Wyithe, S. B., Loeb, A., et al., 2002, ApJ, 581, 886
- [2003] Wyithe, S. B., Loeb, A., et al., 2003, ApJ, 586, 693
- [2004] Wyithe, S. B., Loeb, A., et al., 2004, Nature, 427, 815
- [2006] Wyithe, S. B., Padmanabhan, T., et al., 2006, MNRAS 366, 1029
- [2006] Wyithe, S. B., Cen, R., et al., 2006, astro-ph/0602503
- [2004] Yoshida, N., Bromm, V., Hernquist, L., et al., 2004, ApJ 605, 579
- [2002] Yu, Q., Tremaine, S., et al., 2002, MNRAS, 335, 965
- [2005] Zahn, O., et al, 2005, ApJ 630, 657
- [2006] Zahn, O., et al, 2006, to appear. Presented at Aspen Winter Meeting Jan. 2006.
- [2004] Zaldarriaga, M., Furlanetto, S., Hernquist, L., et al., 2005, ApJ 608, 622

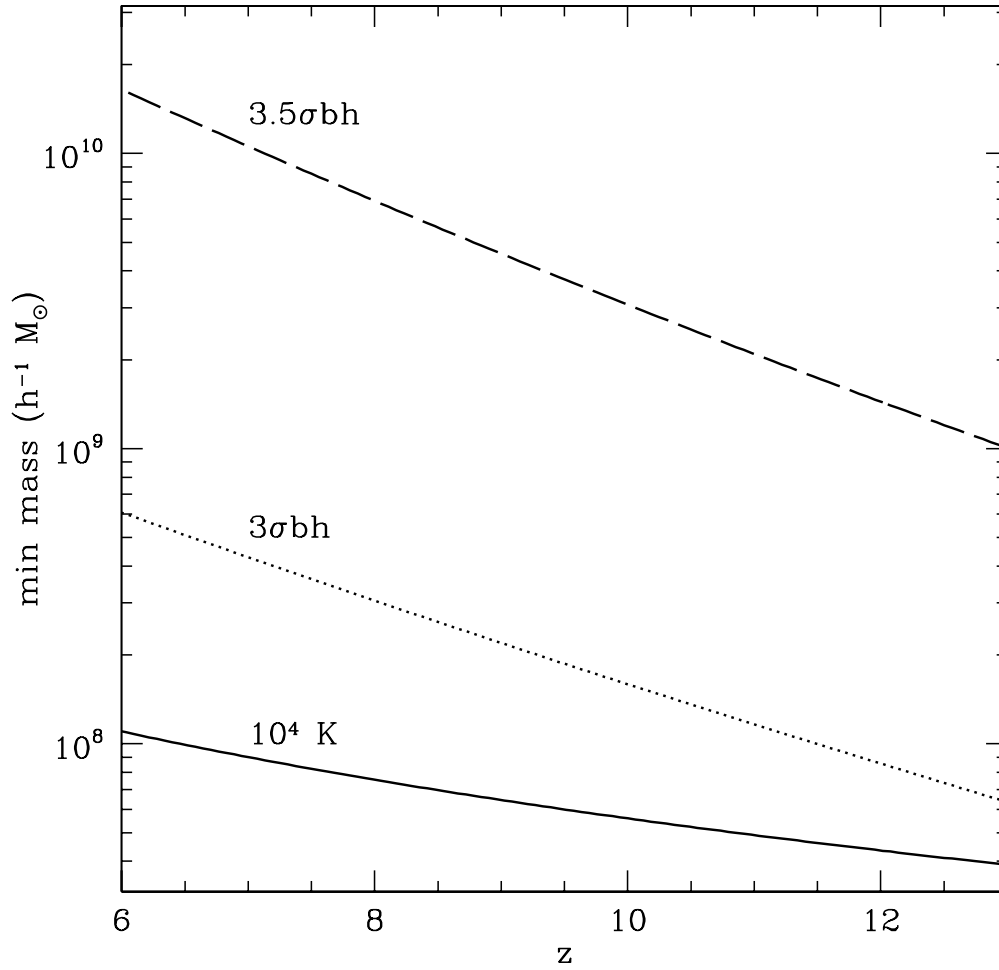


Figure 1: Minimum halo masses used as a function of redshift. The lowest solid line is the mass of a $10^4 K$ halo. The middle dotted line and upper dashed line show the minimum mass for a halo to contain a black hole, choosing 3 or 3.5 halos at $z = 24$ to host black holes, see appendix for details.

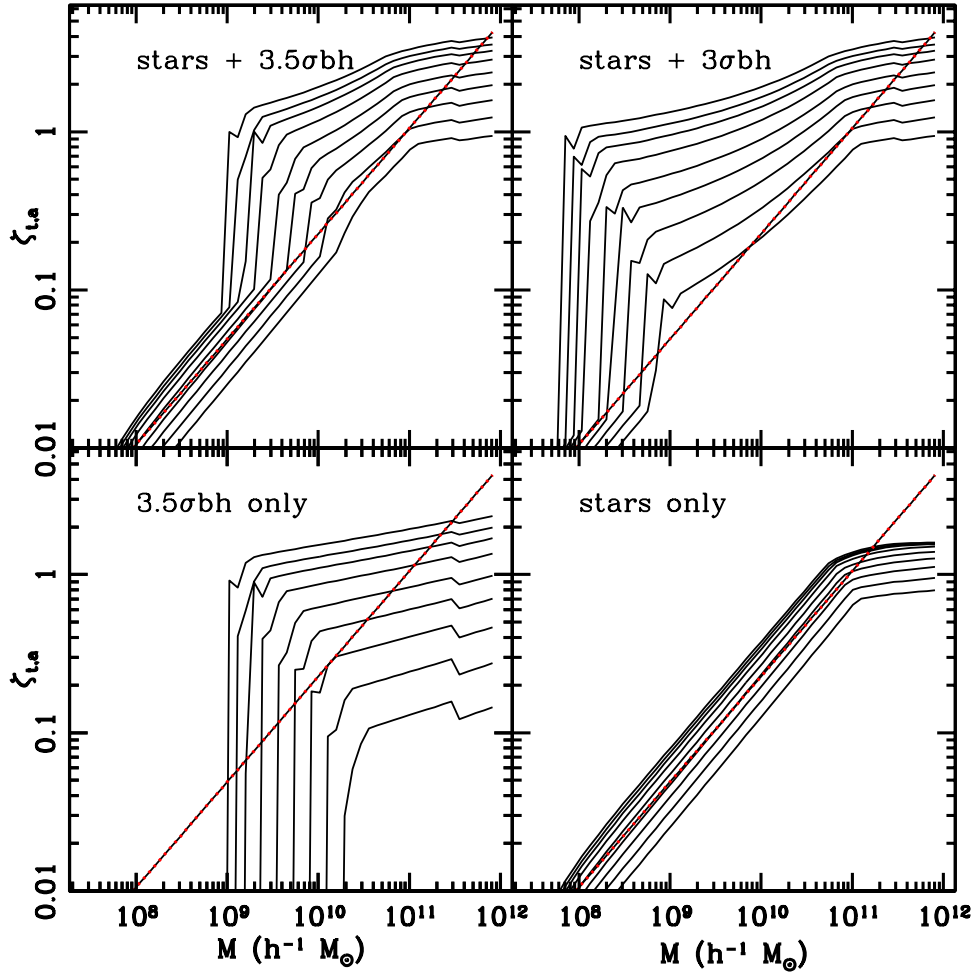


Figure 2: Redshift and mass dependence of $t_{ja}(m)$, lines are $z = 5.9; 7.1; 8.0; 9.0; 10.2; 11.2; 11.9; 12.6; 13.4$, bottom to top (mergers are more common in the past, increasing photon production and thus $t_{ja}(m)$). Top left: stars and 3.5 black holes, top right: stars and 3 black holes. Bottom left: 3.5 black holes only. Bottom right, stars only. The dotted line in each case is the slope that would arise from a time independent $m^{2=3}$ power law. Mergers steepen this power law dependence slightly ($m^{0.7}$) at every redshift.

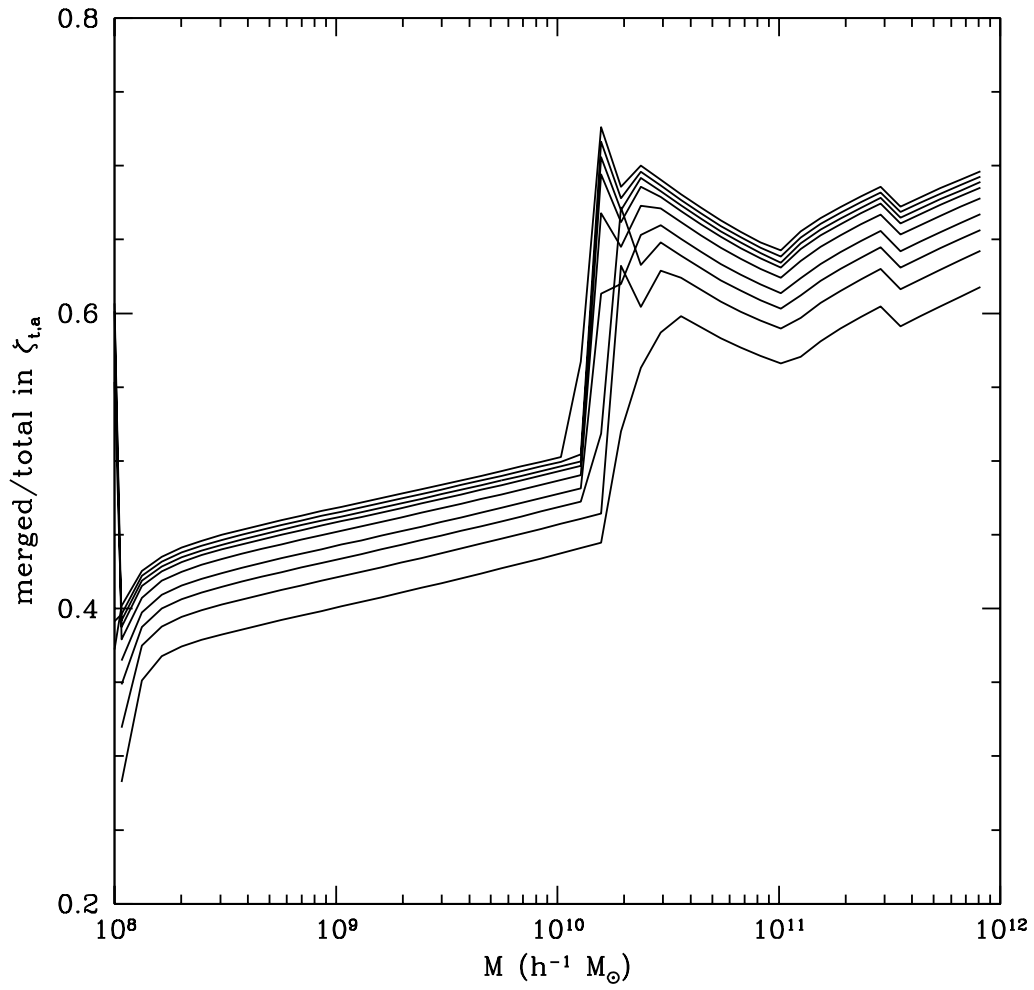


Figure 3: Ratio of photon production rates: merger-produced/ (merger produced and quiescent) as a function of mass, for $z = 5.9; 7.1; 8.0; 9.0; 10.2; 11.2; 11.9; 12.6; 13.4$, bottom to top. The small wiggle in m ediate above the sharp rise is a numerical artifact.

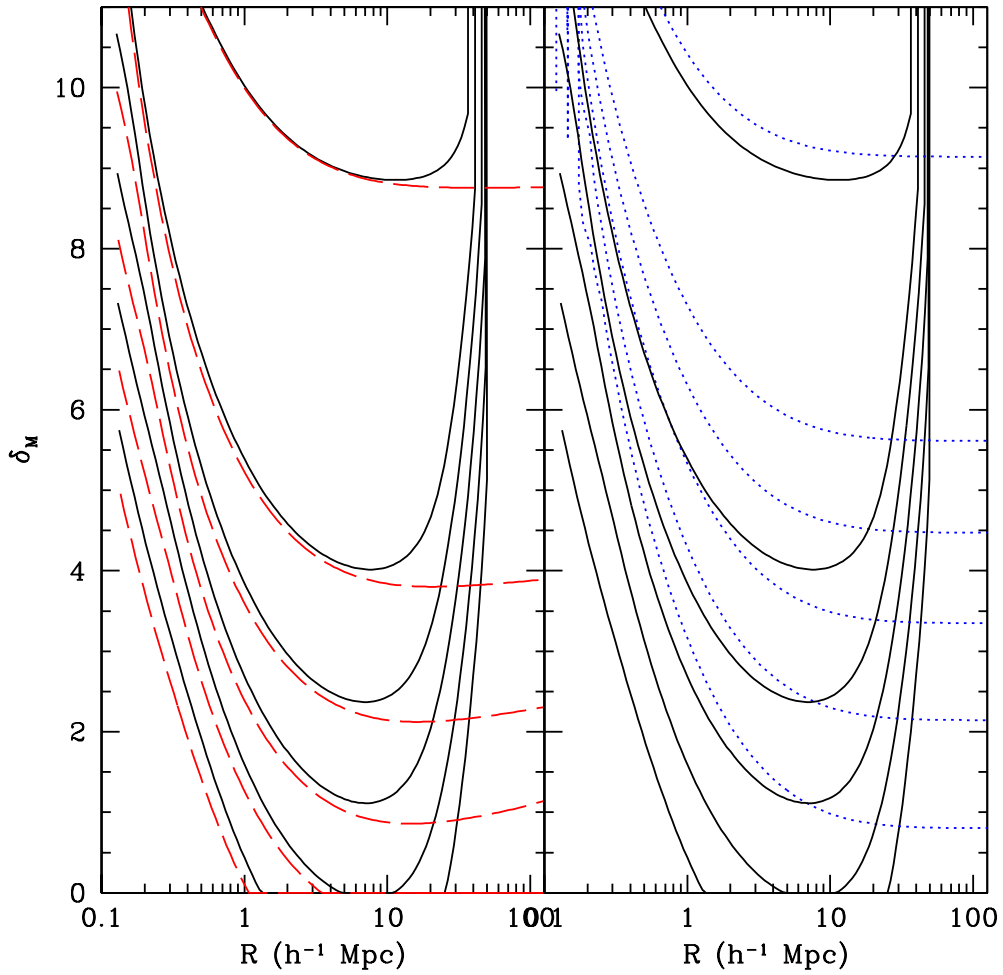


Figure 4: The barriers δ_M found at $z = 7; 8; 9; 10; 11; 11.9$ for our fiducial model. The solid lines (left and right) use m_{inhalo} recombination (eqn. 17 in text), the dashes (left) use M_{HR} recombination (eqn. 15), and the dots (right) use M_{IPS} recombination (eqn. 18).

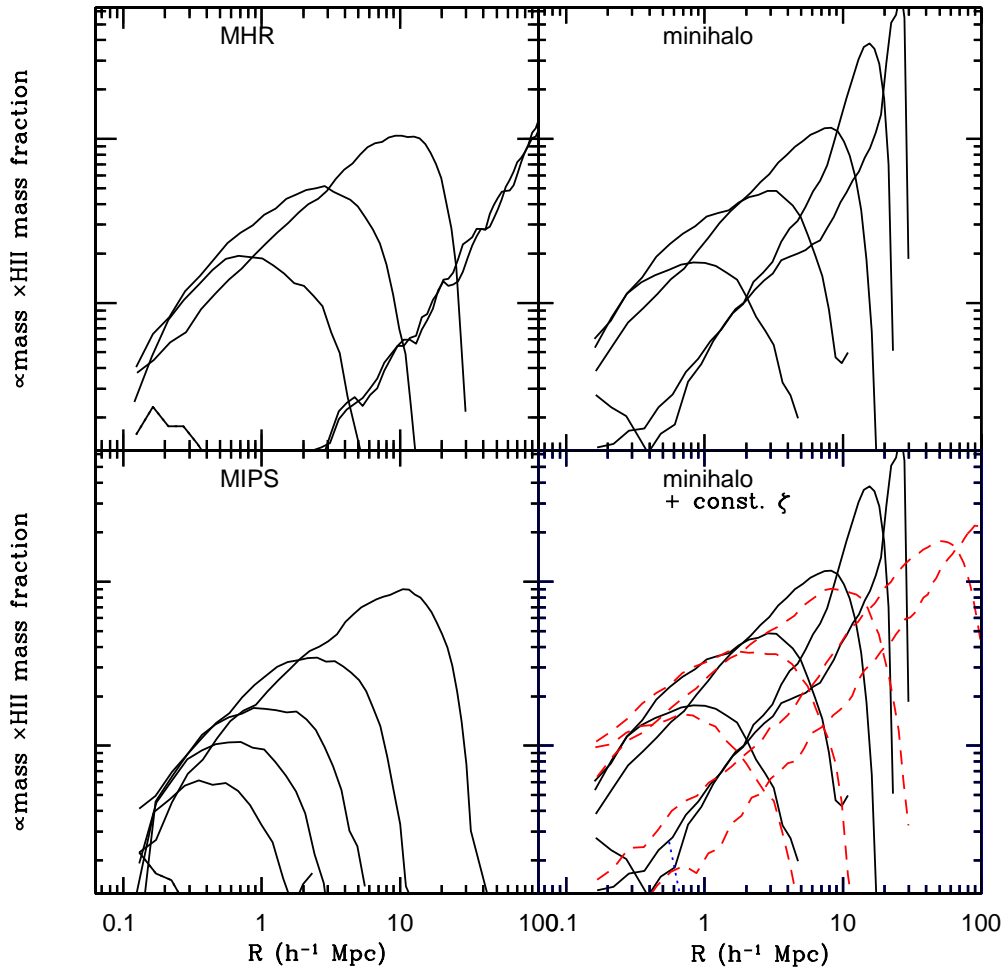


Figure 5: Mass weighted ionized mass fraction as function of R for different redshifts (11.9,11,10,9,8,7) top left and right and bottom left, with the three recombination prescriptions. The curves are weighted by the global ionization fraction at that time (x_i), the smallest curves are at the earliest time. The MHR recombinations are weakest and thus result in the largest bubbles, extending at late times to sizes where many other concerns arise as to interpretation of the model. At bottom right, the minihalo recombination model is shown again (solid line) along with a time independent $\zeta \propto m^{-2=3}$ model (below m_{ref}) having the same x_i at each redshift (dashed line). The time independent models have comparable central values of R for high redshifts and low ionization fractions, i.e. at early times when recombinations aren't very important. Generally their radial distributions are wider as their recombinations are only implicit.

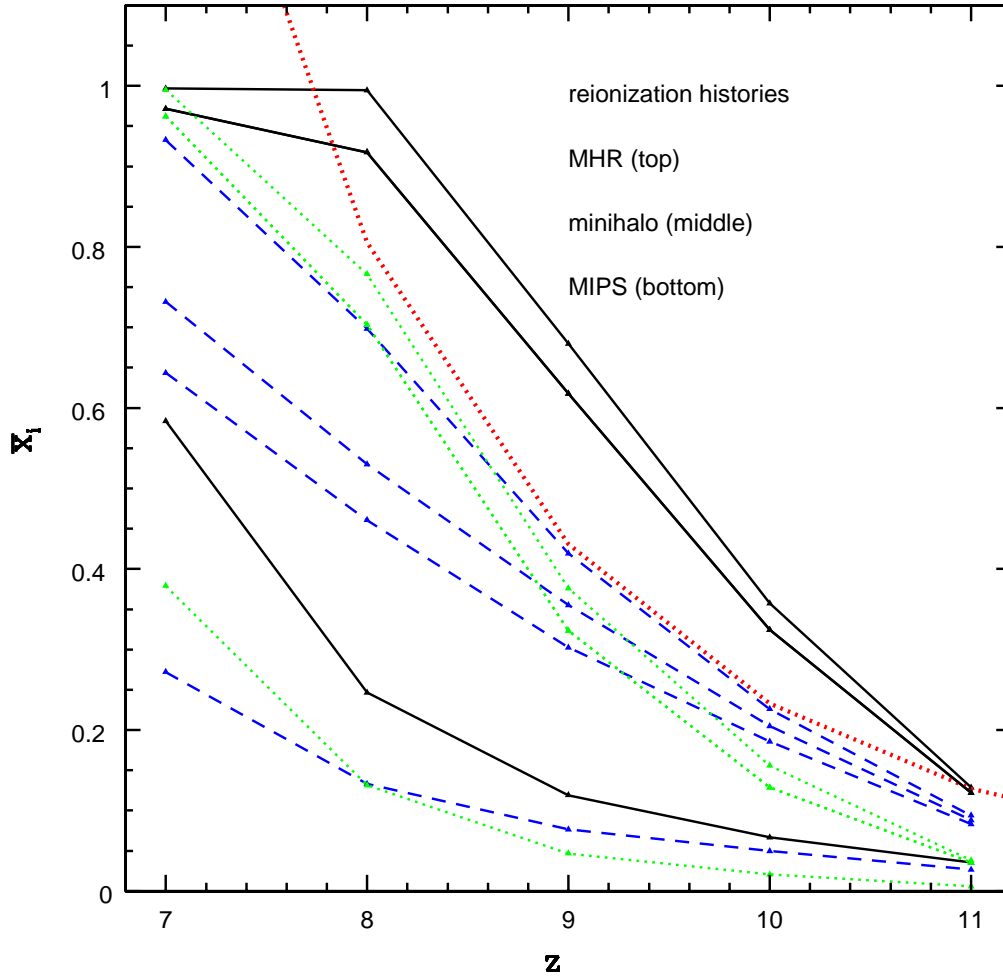


Figure 6: x_i for different redshifts starting with $x_i = 10^{-3}$ at $z = 12$, for MHR, minihalo, and MIPS reionization. The heavy dotted line is the ionization fraction for a constant $\langle n \rangle = m^{2=3}$ model. The short dashed and dotted lines correspond to the models without stars and black holes respectively. For all of the line trios, MHR/minihalo/MIPS recombinations are the top/middle/bottom lines. The minihalo (center) lines are shown for two different Monte Carlo runs to illustrate the run to run scatter.

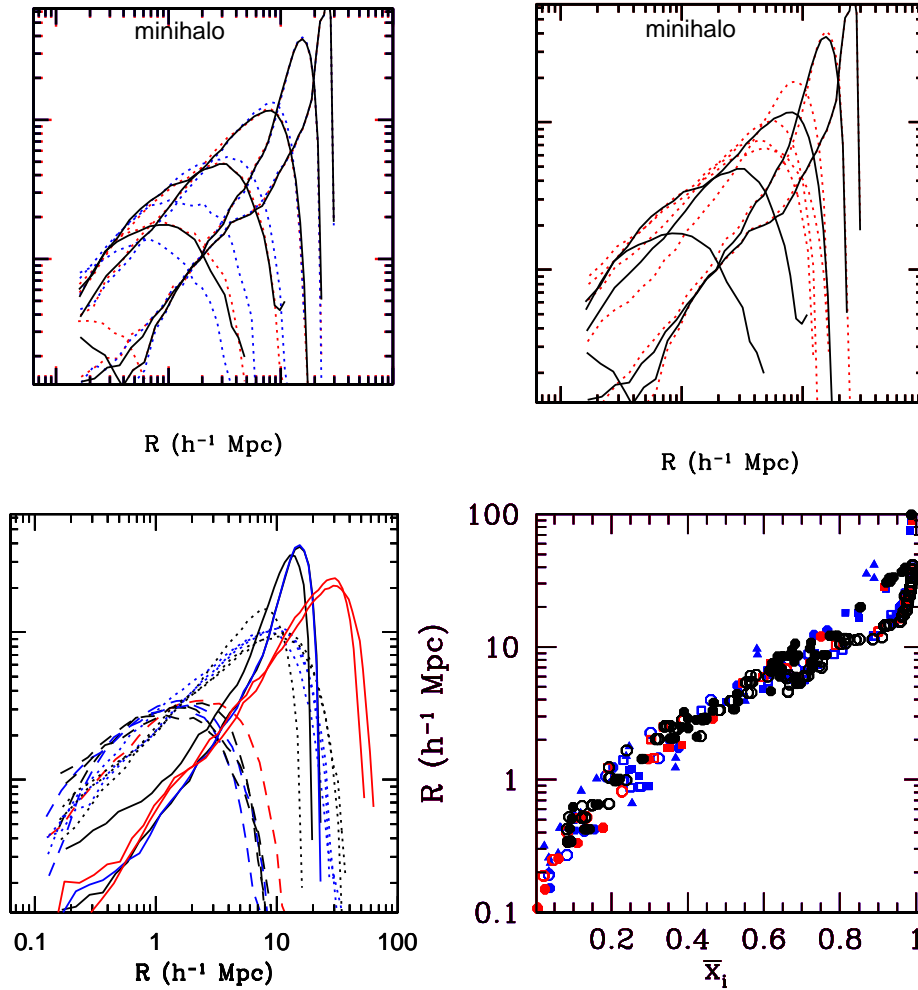


Figure 7: Variations due to different modeling assumptions. Top left and right: initial condition dependence for minihalo recombination case. At left, initial ($z = 12$) $x_i = 10^{-3}$ (solid), 10^{-2} (dots), 10^{-1} (dots), for $z = 11.9; 11; 10; 9; 8; 7$. At right initial $z = 12$ $x_i = 10^{-3}$ (solid), 0.5 (dots), for the same redshifts. Bottom left: full distributions for models with x_i 0.24 (dashed), 0.66 (dotted), 0.91 (solid). The $x_i = 0.91$ models with MHR recombination are peaked at larger R . Bottom right: R_c as a function of x_i is shown for all the models to illustrate trends and model to model scatter. Filled symbols are MHR (triangle) and MIPS (square/octagon) recombinations, open symbols are minihalo recombinations.

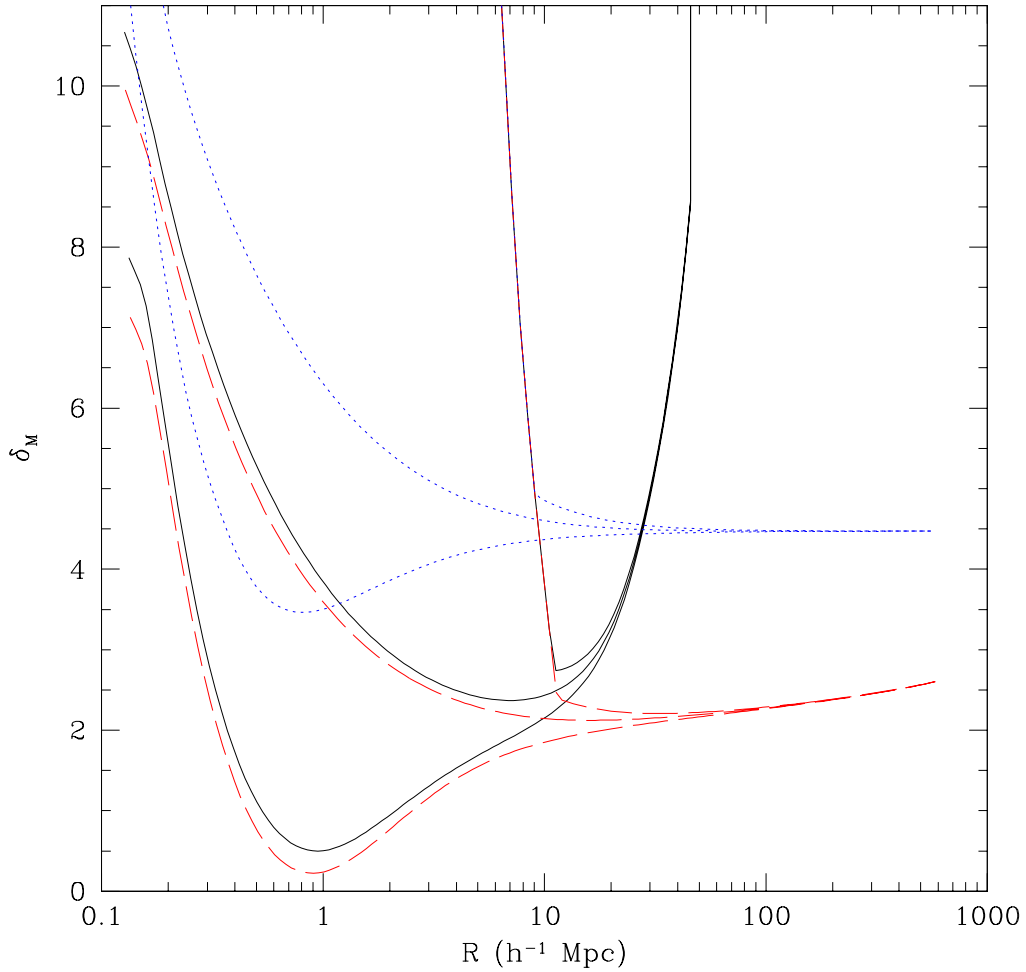


Figure 8: Barriers at $z = 10$ with scatter for the fiducial model. The central line is the mean, lines above and below are ± 1 scatter in the time integral of $\tau_{\gamma a}$ (m) as using the replacement of equation 43. The solid/dashed/dotted lines are mini halo, MHR, MIPS recombination respectively. The scatter to fewer photons results in a larger bubble size: a larger volume is needed in order to enclose a sufficient number of sources.

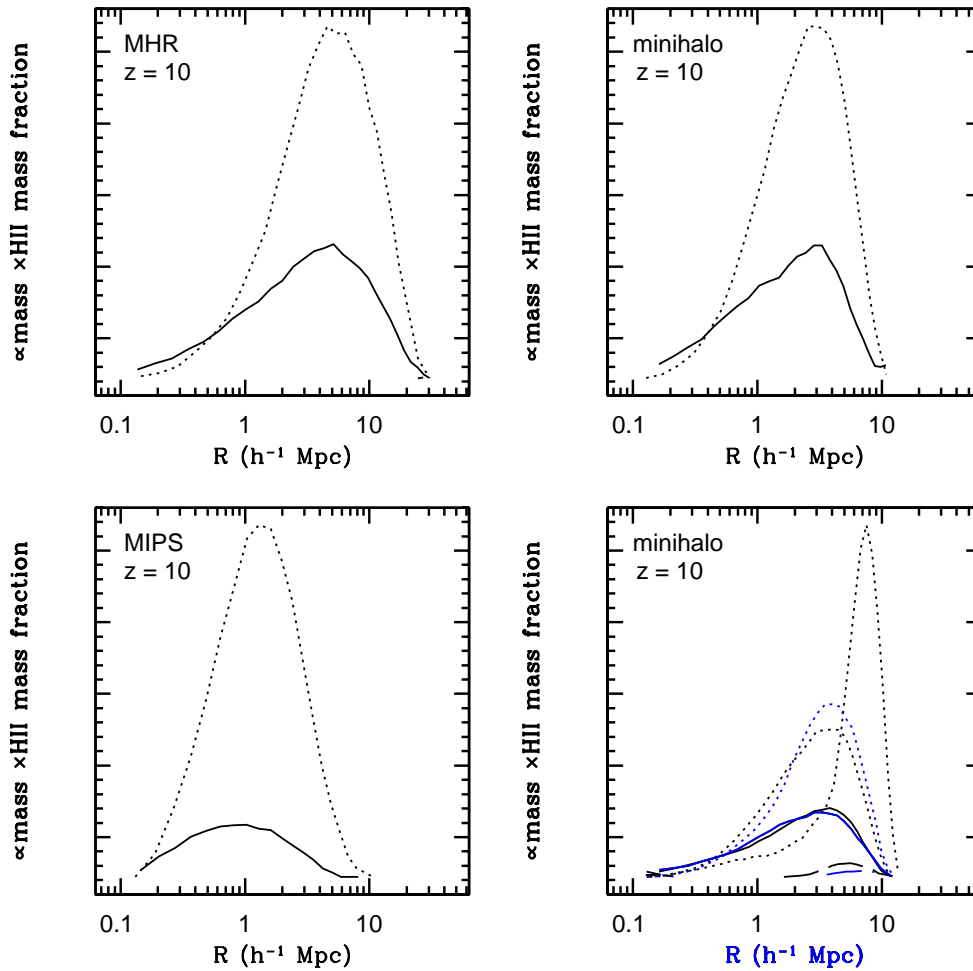


Figure 9: Top left to right and bottom left: Radii at $z = 10$ and their one sigma scatter up and down for our fiducial case for MHR ($x_i = 0.35$), minihalo ($x_i = 0.32$), and MIPS ($x_i = 0.06$) recombination. Bottom right: 3 estimates for scatter at $z=10$ for a model with $x_i(z=12) = 0.14$: starting at $z = 16$, starting at $z = 12$ with usual scatter and starting at $z = 12$ doubling the usual scatter. Solid lines are the mean, dashed lines are scatter to fewer photons, dotted are scatter to more photons. The highest scatter is due to the model with initial conditions set at $z = 16$, including mergers over a longer period of time increases the scatter.

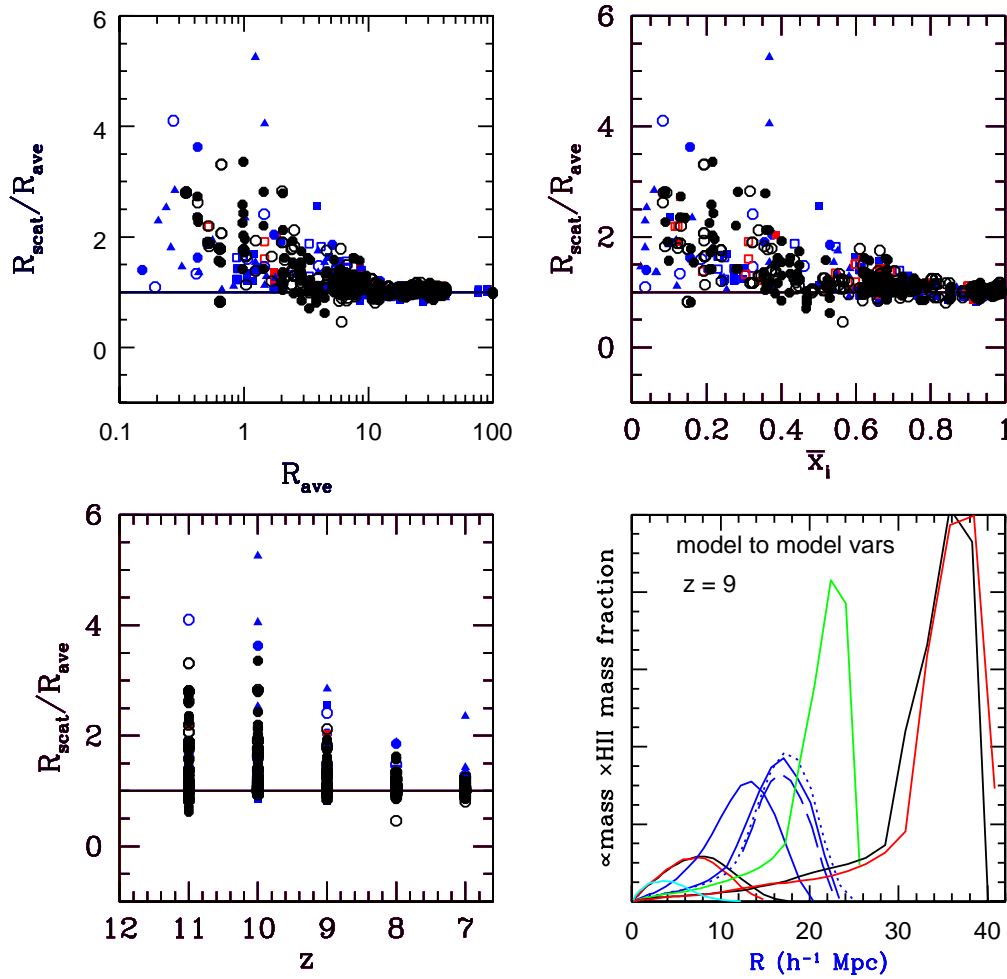


Figure 10: Top left: The ratio $R_{\text{scat}}/R_{\text{ave}}$ amongst several models as a function of R_{ave} . Top right: The range of the mean value of R_c as a function of \bar{x}_i . Bottom left: $R_{\text{scat}}/R_{\text{ave}}$ as a function of redshift. For all three of these, models with $R_c > 100$ are not shown. Filled symbols are MHR (triangle) and MIPS (square/octagon) recombinations, open symbols are minihalo recombinations. Squares are for $n = 1.05$ models, $f_{\text{esc}} = 4f_{\text{esc, ref}}$, $\Omega_b h^2 = 0.0225$, octagons are for the fiducial model with varied initial conditions, including an initial condition set at $z = 16$, and stars only and 3.5 black holes only. Bottom right: many different models are shown at $z = 9$. Left to right (smallest to biggest when there is overlap): fiducial model, $\Omega_b h^2 = 0.0225$, the fiducial model, $n = 1.05$, $f_{\text{esc}} = 4f_{\text{esc, ref}}$ (with scatter), 3 black holes, $\Omega_b h^2 = 0.035$ black holes, $\Omega_b h^2 = 0.03$ black holes. Note the scale for R is linear for this plot.

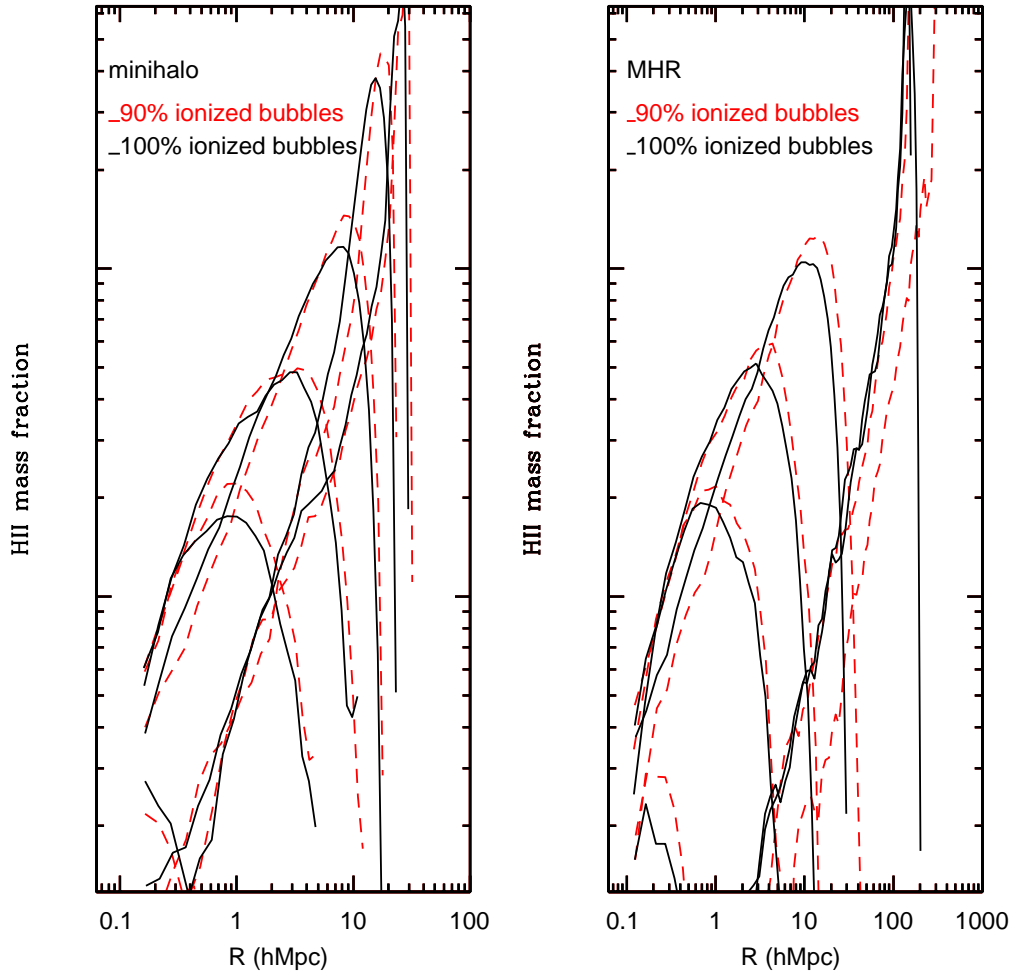


Figure 11: Mass weighted mass fraction in bubbles as function of radius for bubbles which are 100% ionized (solid) and 90% ionized (dashed) at redshifts 11.9, 11, 10, 9, 8, 7 (lowest to highest curves) for minihalo and MHR recombinations (left and right). The effects of changing between fully ionized to 90% ionized bubbles does not change the distribution as a function of radius that much except at large ionization fraction. Note the radial scale for MHR recombinations is much larger.